

# UC Davis

## UC Davis Previously Published Works

### Title

Investigations into hydrogen sulfide-induced suppression of neuronal activity in vivo and calcium dysregulation in vitro

### Permalink

<https://escholarship.org/uc/item/2374x3r2>

### Journal

Toxicological Sciences, 192(2)

### ISSN

1096-6080

### Authors

Kim, Dong-Suk  
Pessah, Isaac N  
Santana, Cristina M  
et al.

### Publication Date



2023-04-17

### DOI

10.1093/toxsci/kfad022

Peer reviewed

# Investigations into hydrogen sulfide-induced suppression of neuronal activity *in vivo* and calcium dysregulation *in vitro*

Dong-Suk Kim,<sup>1</sup> Isaac N. Pessah <sup>1</sup>, Cristina M. Santana,<sup>2,3</sup> Benton S. Purnell <sup>4,5</sup>, Rui Li,<sup>4</sup> Gordon F. Buchanan,<sup>4</sup> Wilson K. Rumbelha<sup>1\*</sup>

<sup>1</sup>Department of Molecular Biosciences, School of Veterinary Medicine, University of California, Davis, Davis, California 95616, USA

<sup>2</sup>VDPAM, College of Veterinary Medicine, Iowa State University, Ames, Iowa 50011, USA

<sup>3</sup>MRI Global, Kansas City, Missouri 64110, USA

<sup>4</sup>Department of Neurology, Iowa Neuroscience Institute, Carver College of Medicine, University of Iowa, Iowa City, Iowa 52246, USA

<sup>5</sup>Department of Nerosurgery, Robert Wood Johnson Medical School, Rutgers University, Piscataway, New Jersey 08854, USA

\*To whom correspondence should be addressed at Department of Molecular Biosciences, School of Veterinary Medicine, University of California, Davis, 1089 Veterinary Medicine Drive, Davis, CA 95616, USA. E-mail: wkrumbelha@ucdavis.edu.

## Abstract

Acute exposure to high concentrations of hydrogen sulfide (H<sub>2</sub>S) leads to sudden death and, if survived, lingering neurological disorders. Clinical signs include seizures, loss of consciousness, and dyspnea. The proximate mechanisms underlying H<sub>2</sub>S-induced acute toxicity and death have not been clearly elucidated. We investigated electrocerebral, cardiac, and respiratory activity during H<sub>2</sub>S exposure using electroencephalogram (EEG), electrocardiogram, and plethysmography. H<sub>2</sub>S suppressed electrocerebral activity and disrupted breathing. Cardiac activity was comparatively less affected. To test whether Ca<sup>2+</sup> dysregulation contributes to H<sub>2</sub>S-induced EEG suppression, we developed an *in vitro* real-time rapid throughput assay measuring patterns of spontaneous synchronized Ca<sup>2+</sup> oscillations in cultured primary cortical neuronal networks loaded with the indicator Fluo-4 using the fluorescent imaging plate reader (FLIPR-Tetra<sup>®</sup>). Sulfide >5 ppm dysregulated synchronous calcium oscillation (SCO) patterns in a dose-dependent manner. Inhibitors of NMDA and AMPA receptors magnified H<sub>2</sub>S-induced SCO suppression. Inhibitors of L-type voltage-gated Ca<sup>2+</sup> channels and transient receptor potential (TRP) channels prevented H<sub>2</sub>S-induced SCO suppression. Inhibitors of T-type voltage-gated Ca<sup>2+</sup> channels, ryanodine receptors, and sodium channels had no measurable influence on H<sub>2</sub>S-induced SCO suppression. Exposures to >5 ppm sulfide also suppressed neuronal electrical activity in primary cortical neurons measured by multielectrode array (MEA), an effect alleviated by pretreatment with the nonselective TRP channel inhibitor, 2-aminoethoxydiphenylborate (2-APB). 2-APB also reduced primary cortical neuronal cell death from sulfide exposure. These results improve our understanding of the role of different Ca<sup>2+</sup> channels in acute H<sub>2</sub>S-induced neurotoxicity and identify TRP channel modulators as novel structures with potential therapeutic benefits.

**Keywords:** hydrogen sulfide; neurotoxicity; *in vitro* models; calcium dysregulation; transient receptor potential; L-type calcium channel

Hydrogen sulfide (H<sub>2</sub>S), an invisible gas with a rotten egg smell, is an occupational environmental toxicant (Rumbelha *et al.*, 2016). It is the second most common cause of fatal gas exposures in workplaces (Guidotti, 2015). Recently, H<sub>2</sub>S gained attention for nefarious uses in chemical terrorism and in suicide (Binder *et al.*, 2018; Morii *et al.*, 2010). H<sub>2</sub>S is also endogenously produced at low concentrations in multiple organs, including the brain, serving multiple physiological functions in vertebrates. It is naturally synthesized from the amino acids, L-cysteine, and L-cystathionine, catalyzed by multiple enzymes including cystathionine-β-synthase, cystathionine-γ-lyase, and 3-mercaptopyruvate sulfur transferase (Polhemus and Lefer, 2014).

Acute exposure to high concentrations of H<sub>2</sub>S induces severe neurotoxicity (Anantharam *et al.*, 2017a,b, 2018; Guidotti, 2010; Kim *et al.*, 2018, 2019; Rumbelha *et al.*, 2016; Snyder *et al.*, 1995; Tvedt *et al.*, 1991b). At concentrations higher than 500 ppm, H<sub>2</sub>S

causes apnea, seizures, coma, and death (Guidotti, 2015; Rumbelha *et al.*, 2016). Most deaths occur at the location of exposure (Santana Maldonado *et al.*, 2022). Among survivors, acute H<sub>2</sub>S exposure often induces delayed neurological sequelae including nausea, persistent headache, movement disorders, impaired memory, amnesia, psychosis, anxiety, depression, sleeping disorders, and coma. Some cases progress to prolonged vegetative states (Rumbelha *et al.*, 2016; Tvedt *et al.*, 1991a; Wasch *et al.*, 1989). Murine and porcine models of H<sub>2</sub>S poisoning exhibit seizure activity and loss of consciousness (Anantharam *et al.*, 2017a,b, 2018; Kim *et al.*, 2018, 2019; O'Donoghue, 1961). Seizure activity has a high correlation with loss of consciousness in H<sub>2</sub>S-exposed mice (Anantharam *et al.*, 2017a). The frequency and severity of seizure activity varies among mice, although seizure severity predicts shorter survival time (Anantharam *et al.*, 2017a, 2018; Kim *et al.*, 2018, 2019). Interestingly, preventing seizures

with an anticonvulsant agent prolongs the survival of mice during H<sub>2</sub>S exposure (Anantharam et al., 2018). Victims of acute H<sub>2</sub>S poisoning also develop pulmonary edema (Tanaka et al., 1999) and heart failure (Sastre et al., 2013). Results from some animal models indicate cardiac arrest after acute sodium hydrosulfide (NaHS) exposure (Haouzi et al., 2015).

Despite this knowledge, it remains unclear what organ(s) primarily mediates H<sub>2</sub>S-induced physiological dysfunction leading to death and which are second order sequelae of H<sub>2</sub>S exposure. For example, respiratory arrest will eventually precipitate cardiac arrest as a secondary outcome, but the inverse is also true. Likewise, cardiac and respiratory arrest can both elicit cerebral hypoxia which can trigger electrocerebral suppression and, in extreme cases, seizures; however, seizures and hypoxia can also elicit cardiac and respiratory dysfunction. Determining which factors are initiating the H<sub>2</sub>S cascade necessitates simultaneous respiratory, cardiac, and electrocerebral recordings under tightly controlled experimental conditions. Moreover, the molecular mechanisms underlying H<sub>2</sub>S-induced neurotoxicity and death are poorly understood.

It is widely reported that H<sub>2</sub>S inhibits cytochrome c oxidase enzyme in mitochondria; however, this alone does not explain the broad spectrum of toxic effects from knockdown and coma, to development of vegetative states (Anantharam et al., 2017a,b, 2018; Guidotti, 2015; Kim et al., 2018, 2019; Ng et al., 2019; Snyder et al., 1995; Tvedt et al., 1991a,b). Transcriptomic and proteomic studies of the inferior colliculus in H<sub>2</sub>S-exposed mice showed that H<sub>2</sub>S induces dysregulation of multiple biological pathways including calcium homeostasis, oxidative stress, immune response, and neurotransmitters (Kim et al., 2018, 2019).

Calcium homeostasis is important for virtually all neuronal functions. Synchronous calcium oscillations (SCOs) are ubiquitous signaling mechanisms whose frequency and amplitude encode information in both individual neurons (eg, regulating physiologic metabolic and transcriptional responses) and at the level of networks (eg, regulating synaptic connectivity and circadian rhythms) (Alford and Alpert, 2014; Cavieres-Lepe and Ewer, 2021; Tokumitsu and Sakagami, 2022). SCO patterns encode frequency and amplitude signals that provide a means to control a wide range of cellular physiological functions (Smedler and Uhlen, 2014; Sneyd et al., 2017). Dysregulation of SCO patterns has been reported in Alzheimer's disease (Santos et al., 2009) and Huntington's disease (Glaser et al., 2021). Various environmental toxicants have also been reported to disrupt SCO in neuronal cell cultures (Cao et al., 2014, 2017; Zheng et al., 2019).

Primary cortical neuronal coculture (PCN) displays spontaneous electrical spike activity that form synchronized and desynchronized field potentials as the PCN develops (Cao et al., 2014; Zheng et al., 2019). This PCN model exhibits spontaneous SCOs which are driven by spontaneous electrical spike activity (Cao et al., 2012, 2014; Muramoto et al., 1993; Robinson et al., 1993; Zheng et al., 2019). SCOs are shown to be strongly related to seizure activity in an *in vitro* epileptic model (Sombati and Delorenzo, 1995). There are several types of Ca<sup>2+</sup> channels in the brain that mediate physiological, pharmacological, and toxicological responses (Table 1). However, whether H<sub>2</sub>S alters SCO patterns and, if so, the channels contributing to dysfunction have not been investigated.

The present study uses an *in vivo* mouse model of inhaled H<sub>2</sub>S to measure brain electroencephalogram (EEG), electrocardiogram (EKG), and plethysmography to determine temporal changes in brain, heart, and lung, respectively, during H<sub>2</sub>S exposure. We identify suppression of brain electrical activity as the proximal

**Table 1.** Select calcium channels in the brain, their specific inhibitors, and location

Ca <sup>2+</sup> channel	Inhibitor	Channel location
AMPA	perampanel	Cell membrane
NMDAR	mK-801	Cell membrane
L-type VGCC	nifedipine	Cell membrane
L-type VGCC	nimodipine	Cell membrane
T-type VGCC	ethosuximide	Cell membrane
TPC	2-APB	Endoplasmic reticulum or cell membrane
Ryanodine receptor	dantrolene	Endoplasmic reticulum

effect of H<sub>2</sub>S intoxication preceding reduced pulmonary function and death. In combination with our prior knowledge that H<sub>2</sub>S causes Ca<sup>2+</sup> dysregulation in brain and the important role of Ca<sup>2+</sup> signaling in regulating neurological functions, we developed an *in vitro* PCN cell culture model to further test our *in vivo* findings of acute H<sub>2</sub>S exposure. The use of FLIPR and multielectrode array (MEA) assays with the PCN culture model provides new information about how H<sub>2</sub>S alters neuronal Ca<sup>2+</sup> signaling and the mechanisms responsible.

## Materials and methods

### Reagents

Poly-L-Lysine (PLL), Fluo-4 AM, bovine serum albumin (BSA), cytosine β-D-arabinofuranoside (ARA-C), MK-801, nifedipine, nimodipine, 2-aminoethoxydiphenylborate (2-APB), and dantrolene were purchased from Sigma Aldrich (St. Louis, MO). Perampanel and ethosuximide were generously gifted from Dr. Michael Rogawski, University of California at Davis (UC Davis). Neurobasal media, HEPES, penicillin-streptomycin, B-27 Plus, GlutaMAX, fetal bovine serum (FBS), Flu-4 AM, calcein AM, and Hoechst 33342 were purchased from Thermo Fisher Scientific (Waltham, MA).

### Animals

Animal use was approved by the Institutional Animal Care and Use Committee (IACUC) of UC Davis or the University of Iowa, Iowa City. Animals were treated humanely and handled with care in accordance with IACUC guidelines.

### EEG, EMG, and EKG surgery

C57BL/6J mice were purchased from Jackson Laboratories (000664; Bar Harbor, ME). Seven- to 8-week-old male C57BL/6J mice were housed at room temperature of 20–22°C with a 12:12 h light dark cycle. Food (NIH-31 Mouse Diet) and water were available *ad libitum*. EEG and EKG electrodes were implanted as previously described (Muramoto et al., 1993). Briefly, mice were anesthetized under 1% isoflurane and skull surface was exposed and prepared. The headmount was then secured onto the skull aligning its middle with sagittal suture and the front 2 holes were in front of the coronal suture, while the back 2 holes were in front of the lambdoid suture. Four pilot holes were bored with a 23G hypodermic needle. The screws were coated with silver epoxy and were driven into the holes acting as EEG electrode. Two stainless steel wires extended from the headmount were buried under cervical muscle to collect electromyography (EMG) signals. The headmount was then secured using dental cements. Mice were allowed to recover for at least 1 week before experimentation.

## EEG and EKG recording

EEG and EKG signals were acquired and processed as previously described (Purnell et al., 2017). Briefly, the preamplifier (8202-SL; Pinnacle Technology Inc.) was attached to the exposed plug on the implanted EEG headmount. EKG leads (MS303-76; Plastics One, Roanoke, VA) were implanted during the same surgery in the left chest wall and right axilla in a modified lead II configuration. The preamplifier cord was passed through an airtight gasket in the custom plethysmography chamber and then attached to a 6-channel commutator (no. 8204; Pinnacle Technology Inc.). The signal was passed to a conditioning amplifier (model 440 Instrumentation Amplifier; Brownlee Precision, San Jose, CA). The EEG signals were amplified (100 times), band-pass filtered (0.3–200 Hz for EEG), and digitized (1000 samples/s; NI USB-6008; National Instruments, Austin, TX). The digitized signal was transferred to a desktop computer and recorded using software custom written in MATLAB (R2018b; MathWorks, Natick, MA).

## Whole-body plethysmography

Whole-body plethysmography was employed to measure respiratory parameters during acute H<sub>2</sub>S exposure. Each animal was acclimated to the chamber. Baseline breathing was recorded for 10 min before exposure to 1000 ppm H<sub>2</sub>S or regular breathing air from pressurized cylinders. The recording chamber was outfitted with an ultralow volume pressure transducer (DC002NDR5; Honeywell International Inc., Morris Plains, NJ) to detect small pressure waves associated with breathing. The signal was amplified (100 times), band-pass filtered (0.3–30 Hz), and digitized before being recorded with a custom MATLAB software and stored on a desktop computer following previously published protocol (Purnell and Buchanan, 2020). Before H<sub>2</sub>S or breathing air exposure, the signal was calibrated by delivering metered breaths (300  $\mu$ l; 150 breaths min<sup>-1</sup>) via a mechanical ventilator (Mini-Vent; Harvard Apparatus) to the recording chamber. Respiratory function parameters including minute ventilation (V<sub>E</sub>), tidal volume (V<sub>T</sub>), and respiratory rate were assessed with MATLAB custom script as previously described (Hodges and Richerson, 2008).

## Exposure paradigm

Mice were acclimated to the air-tight exposure chamber for 1 h twice on different days prior to experimentation. EEG, EKG, and whole-body plethysmography recordings were calibrated before exposure to 1000 ppm H<sub>2</sub>S gas or breathing air from pressurized cylinders. Five minutes of baseline EEG, EKG, and whole-body plethysmography recordings were made before gas exposure. Gas exposure was simulated without an animal twice, while the concentration of H<sub>2</sub>S in the plethysmography chamber was monitored in real-time using a H<sub>2</sub>S sensor (RKI instrument, Union City, CA). EEG, EKG, and breathing of C57BL/6J mice was monitored in real-time using implanted electrodes and the air-tight plethysmography chamber as shown in the exposure paradigm figure (Figure 1A). Mice were continuously exposed to the gas until complete cardiac arrest as assessed by EKG (about 2 h) as the endpoint was mortality for this part of the study. Mice in the control group were exposed to normal breathing air, also from a pressurized cylinder.

## Primary cortical neuron culture (PCN)

Male and female wild type (WT) C57BL/6J mice (000664) were purchased from Jackson Laboratories (Sacramento, CA) and were

housed in the Teaching and Research Animal Care Services facility (TRACS) at the School of Veterinary Medicine, UC Davis with a 12:12 h light and dark cycle. Room temperature and relative humidity were maintained at 22°C and 50  $\pm$  10% respectively. Dissociated cortical neurons with minimal astrocyte composition were cultured as described previously (Cao et al., 2017). Briefly, neurons were dissociated from the cortex of C57BL/6J mouse pups of both sexes on postnatal day 0–1 and maintained in complete Neurobasal media (50 units of penicillin, 50  $\mu$ g/ml streptomycin, 2% [v/v] B-27 Plus, 10 mM HEPES, and 1% [v/v] GlutaMAX) supplemented with 2% FBS. Dissociated cortical neurons were seeded onto the plate precoated with PLL at a density of 1  $\times$  10<sup>5</sup>/well for 96-well plate for fluorescence laser plate reader (FLIPR Tetra; Molecular Devices, Sunnyvale, CA) or MEA plate. The cell culture media was diluted to 2-fold with complete Neurobasal medium the next day. A final concentration of 10 mM ARA-C was added to the culture medium at 36–48 h of culture to prevent astrocyte proliferation. The culture medium was changed every other day by replacing half volume of the culture medium with serum-free complete Neurobasal medium. PCN were maintained at 37°C with 5% CO<sub>2</sub> and 95% humidity until experiment. We used developing primary cortical neurons (PCN) because they express multiple calcium channels and receptors, form neuronal networks, have SCOs, and produce neuronal electrical activity. The use of PCN is advantageous because the protocols to isolate and maintain PCN are well established and because cortex because of size provides the most neurons per individual animal.

## Measurement of synchronous Ca<sup>2+</sup> oscillations

Synchronous Ca<sup>2+</sup> oscillations of the PCN culture were measured using fluorescent labeled calcium indicator and a FLIPR Tetra<sup>®</sup> system as previously described (Cao et al., 2017). This fluorescent plate reader-based Ca<sup>2+</sup> assay allowed measurement of functional Ca<sup>2+</sup> signaling in PCN providing a rapid throughput *in vitro* system to assess the role of various Ca<sup>2+</sup> channels in H<sub>2</sub>S-induced neurotoxicity using various pharmacological probes. Briefly, PCN between day *in vitro* (DIV) 9 and DIV 16 were used. The growth medium was replaced with a dye loading solution (75  $\mu$ l/well) containing 5  $\mu$ M Fluo-4 AM and 0.5% BSA in Neurobasal medium. After incubation for 1 h in the dye loading solution, cells were washed 2 times with Neurobasal medium and once with imaging solution (125 mM NaCl, 5 mM KCl, 2 mM CaCl<sub>2</sub>, 1.2 mM MgCl<sub>2</sub>, 25 mM HEPES, and 6 mM Glucose at pH 7.2). After washing, the cell medium was gently aspirated, and 125  $\mu$ l of imaging solution was then added to the cells. The plate was transferred to FLIPR instrument to measure real-time intracellular Ca<sup>2+</sup> concentration using a fluorescent signal. The fluorophore within the cells was excited at 488 nm, and Ca<sup>2+</sup>-bound Fluo-4 emission was recorded at 535 nm. Baseline recordings of SCO were obtained before addition of the toxicant and/or drug probes using a programmable 96-channel robotic pipetting system. Properties of the SCO, including frequency and amplitude were analyzed using *scipy* module (version 1.7.1) in Python version 3.0 Software script (<https://www.python.org/>). A typical diagram of peak parameters of the normal SCO is shown in Supplementary Figure 1.

## Multielectrode array recordings

Measuring spontaneous neuronal electrical activities using MEA system (Axion BioSystems, Atlanta, GA) was another cell function assay. It was performed as described previously (Cao et al., 2012). Briefly, dissociated PCN were seeded on to 48-well Maestro plates at a density of 1  $\times$  10<sup>5</sup>/well and maintained by changing growth



medium every other day until use on 9–16 DIV. At the time of the experiment, the growth medium was gently aspirated and 125  $\mu$ l Neurobasal medium was added to the cells. The plate was transferred to the MEA instrument prewarmed to 37°C. Cells were incubated on the MEA system for 5 min before measuring basal electrical activity. Cells were pretreated with vehicle or pharmacological drug probes, followed by exposure to H<sub>2</sub>S. The MEA instrument recorded and amplified the raw extracellular electrical signals which were digitized in the Axis software at a rate of 25 kHz and filtered using a Butterworth band-pass filter (cutoff frequency of 300 Hz). The Axis software was used to detect spontaneous electrical events, perform spike analysis, and to export the analyzed data.

### Cell viability assay

Cell viability was performed using ImageXpress<sup>®</sup> Micro (Molecular Devices, San Jose, CA) and cell-permeant dye, calcein AM, according to the manufacture's protocol. Briefly, PCN were grown in precoated 96-well plate with PLL. Primary cortical neuronal/glia coculture DIV 9–16 were exposed to designated concentrations of H<sub>2</sub>S for 40 min at 37°C. At the conclusion of the exposure period, the medium was aspirated and replaced with the growth medium. The H<sub>2</sub>S-exposed PCN were incubated for 72 h at 37°C with change of growth medium after 48 h. Calcein AM was applied to the H<sub>2</sub>S-exposed PCN and incubated for 30 min before taking images of cells using ImageXpress<sup>®</sup> Micro. Hoechst 33342 was used for nuclei staining. Live cell counts were calculated using MetaXpress version 6 (Molecular Devices).

### Data analysis

Data are presented as mean and standard deviation of the mean. SCO peak parameters were normalized to the baseline values, which were compared to the control group. Statistical analyses of SCO peak parameters were performed by Student's *t*-test using Microsoft Excel (Redmond, WA) or ANOVA using scipy statistical module (version 0.12.2) in Python version 3.0 (<https://www.python.org/>). A *p*-value of <.05 was accepted as statistically significant.

## Results

### *In vivo acute H<sub>2</sub>S exposure caused rapid suppression of electrocerebral and respiratory suppression which preceded cardiac dysfunction*

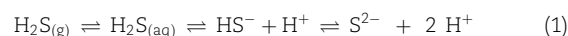
Mice exposed to normal air showed normal patterns of EEG, EKG, and plethysmography similar to the resting biopotentials throughout the observation period including recording epoch 1 and epoch 2 depicted in Figure 1B. Exposure to 1000 ppm H<sub>2</sub>S induced significant disruption in brain and breathing activity starting within recording epoch 1 which became more severe within recording epoch 2 (Figure 1B). Mice exposed to H<sub>2</sub>S exhibited an unstable burst-suppression pattern of EEG (Figure 1B). Recording epoch 1 (Figure 1B) shows that H<sub>2</sub>S-induced suppression of electrocerebral and respiratory suppression started as early as 5–7 min into H<sub>2</sub>S exposure. Thirty-four minutes into exposure (recording epoch 2), suppression of both electrocerebral activity and breathing became prominent (Figure 1B). However, cardiac activity was substantially less strongly impacted. Mice exposed to H<sub>2</sub>S displayed frequent seizure activity which was followed by loss of postural control, profound electrocerebral suppression, and behavioral immobility, presumably due to a loss of consciousness. The duration of electrographic burst/suppression

episodes varied, but typically lasted for a few seconds to about 30 s. H<sub>2</sub>S exposed mice showed clear behavioral seizure activity before loss of consciousness characterized by myoclonus, body jerks, head bobbing, and loss of postural control; however, the cortical EEG traces during this time were not characterized by the high frequency, high amplitude discharges which typically characterized epileptiform discharges. The electrographic activity became progressively weaker as the exposure to H<sub>2</sub>S continued. Most notably, periods of electrographic suppression were frequently accompanied by apnea.

Respiratory suppression began early following the onset of H<sub>2</sub>S exposure and progressively worsened until the animal died (Figure 2). In contrast, severe suppression of cardiac activity did not occur until >30 min after the onset of H<sub>2</sub>S exposure (Figures 2 and 3). Furthermore, the suppression of cardiac activity during the first 10 min of H<sub>2</sub>S exposure was partially recovered (Figures 2 and 3). Given that respiratory suppression was only getting progressively more severe during this time period, it seems likely that the terminal decline in cardiac activity (>30 min following exposure) was the consequence of prolonged hypoxia due to insufficient respiration (Figure 2).

### *H<sub>2</sub>S suppressed synchronous calcium oscillations in primary cortical neuronal networks*

SCOs in neurons play important roles in processing and interpreting sensory information in the central nervous system (Muramoto *et al.*, 1993; Robinson *et al.*, 1993). The effects of H<sub>2</sub>S on SCO in primary cortical neurons (PCN) were examined using a rapid-throughput FLIPR Tetra<sup>®</sup> system (Figure 4). Cultured PCN DIV 9–16 were exposed to H<sub>2</sub>S from Na<sub>2</sub>S, a H<sub>2</sub>S chemical donor. Na<sub>2</sub>S is spontaneously converted to H<sub>2</sub>S in solution under physiological conditions (Equation 1).



In pilot experiments, a broad concentration range of sodium sulfide (Na<sub>2</sub>S), a chemical donor of H<sub>2</sub>S, was prepared in imaging solution to identify the effective concentration-response relationship for use in our *in vitro* studies. In solution, H<sub>2</sub>S dissociates to hydrosulfide (HS<sup>-</sup>). At high pH (pH >12) HS<sup>-</sup> is transformed to sulfide (S<sup>2-</sup>) ion. H<sub>2</sub>S generated from Na<sub>2</sub>S in the imaging solution was measured by adjusting the pH to a high pH (>12) to convert all hydrosulfide to S<sup>2-</sup>. We measured S<sup>2-</sup> as a biomarker of H<sub>2</sub>S concentration in solution using a sulfide ion microelectrode. Changes in S<sup>2-</sup> concentrations over the 60 min for the dose-response study are summarized in Supplementary Figure 2. Results show that the concentrations of S<sup>2-</sup> decreased over the 60 min observation time, in a concentration-dependent manner.

Effects of high-level H<sub>2</sub>S exposure by itself on SCO in PCN are summarized in Figure 4. SCO activity at rest in PCN (Baseline phase) was measured 10 min before exposure to graded concentrations of H<sub>2</sub>S (Figure 4A). During baseline, cultured PCN continuously exhibited baseline patterns of spontaneous SCO activity. Measured parameters included peak count, peak amplitude, peak width, peak rise time, and peak decay time. Exposure to vehicle (control) did not induce any significant changes in SCO peak parameters (Figure 4A). However, addition of H<sub>2</sub>S induced a biphasic effect on the SCO in PCN. Initially, we observed an acute increase in SCO activity within the first 20–30 s, followed by prolonged suppression of SCO (Figure 4A). We named the acute hyper-active SCO phase as Phase 1, and the subsequent prolonged period of suppressed SCO as Phase 2 (Figure 4A). We also

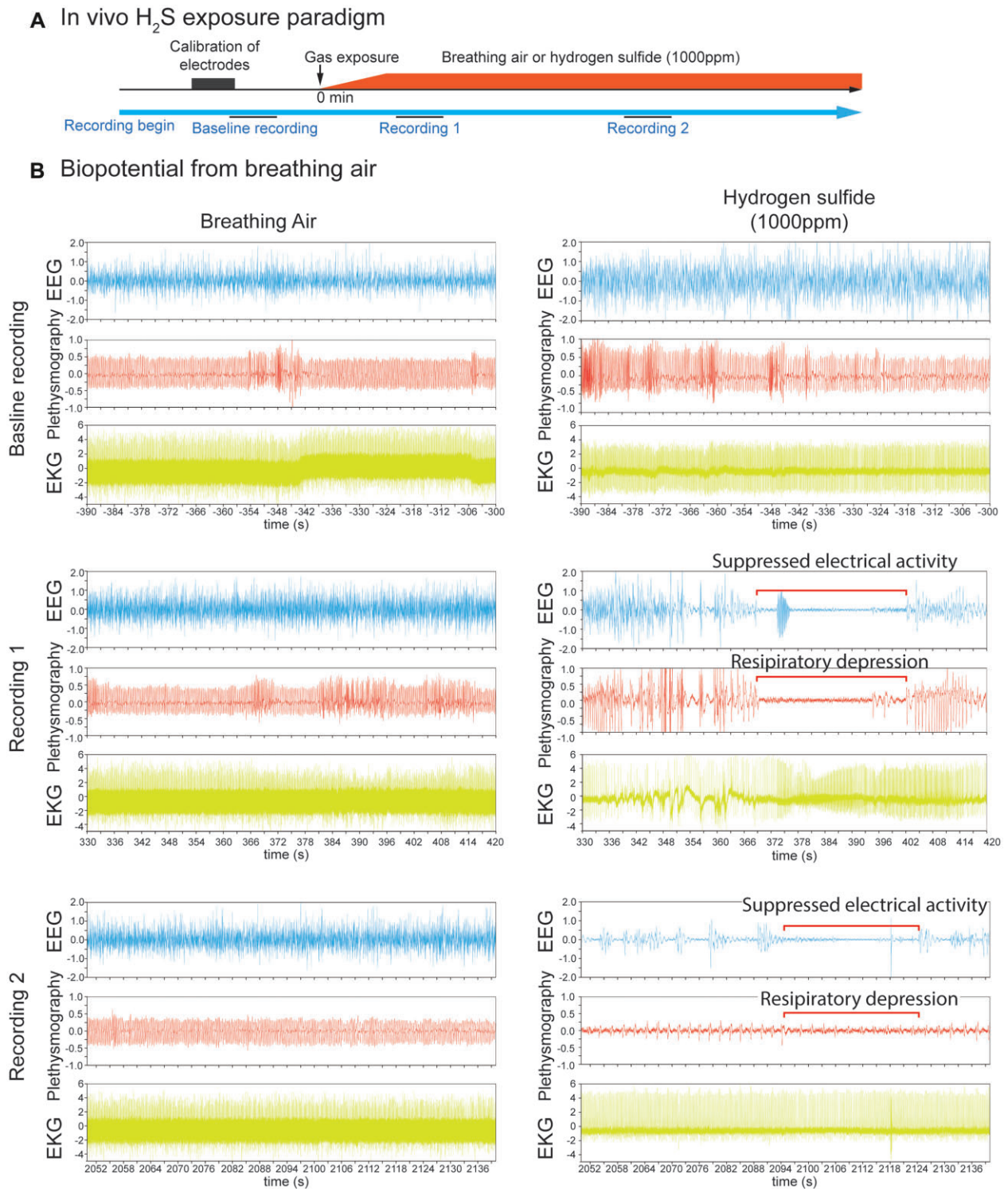


**Figure 1.** *In vivo* H<sub>2</sub>S-induced suppression of brain activity was concomitant with apnea. Mice were preimplanted with electrodes for EEG and EKG. Breathing activity was recorded by plethysmography. *In vivo* H<sub>2</sub>S exposure paradigm was shown in A. After brief calibration of plethysmograph and recordings of biopotentials of baseline activity, mice were exposed to normal breathing air or 1000 ppm H<sub>2</sub>S (B) until death as assessed by EKG. Baseline recordings displayed EEG, EKG, and plethysmography traces of mice at rest. Recording 1 shows 90 s signal recordings at about 5 min from the start of gas exposure, while Recording 2 shows 90 s signal recordings at about 35 min from the start of gas exposure. Recordings 1 and 2 display typical suppression of EEG and plethysmography in H<sub>2</sub>S exposed mice (B). Note the H<sub>2</sub>S-induced electrocerebral suppression and respiratory arrest while cardiac activity persisted (B, Recordings 1 and 2). *N* = 3 mice. Abbreviations: EEG, electroencephalogram; EKG, electrocardiogram; H<sub>2</sub>S, hydrogen sulfide.

noted that suppression of SCO started to recover at about 90 min after the addition of H<sub>2</sub>S. We called this recovery phase Phase 3 (Figure 4A).

These effects of H<sub>2</sub>S were concentration dependent. Statistically significant differences between control and H<sub>2</sub>S exposed cells in each of the 3 phases are summarized in

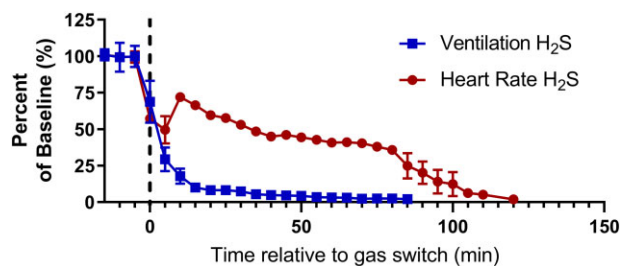


**Figure 2.** Respiratory suppression precedes cardiac suppression during H<sub>2</sub>S exposure. Time series data depicting baseline normalized ventilation (squares, ml/min/g) and heart rate (circles; beats per minute) before and during exposure to 1000 ppm H<sub>2</sub>S. Data are depicted as mean with SEM,  $n = 3$  mice. Baseline was defined as the 15 min prior to H<sub>2</sub>S administration. Dotted line, start of H<sub>2</sub>S exposure. Abbreviations: H<sub>2</sub>S, hydrogen sulfide.

Figures 4B–D. Note that peak count was significantly increased by H<sub>2</sub>S in Phase 1 (Figure 5Bi) but significantly suppressed in Phases 2 (Figure 4Ci) and 3 (Figure 4Di) compared to the respective Phases in vehicle control. H<sub>2</sub>S-exposed PCN showed significantly decreased SCO peak width, peak rise time, and peak decay time in Phase 1 (Figs. 4Bii, 4Biii, and 4Biv). These effects of H<sub>2</sub>S were reversed (increased) in peak width, peak rise time, and peak decay time in Phases 2 and 3 (Figs. 4C and 4D). Effects of H<sub>2</sub>S on SCO in Phase 2 were reminiscent of comma/depression phenotype in Recording 2 in Figure 1C of the H<sub>2</sub>S exposed mice *in vivo*.

#### Transient receptor potential channel blocker, 2-APB, prevents H<sub>2</sub>S-induced suppression of SCO

Store-operated Ca<sup>2+</sup> entry plays important roles in regulating intracellular Ca<sup>2+</sup> in many eukaryotic cells, including neurons (Grudt et al., 1996). Of relevance to potential mechanisms contributing to high concentrations of H<sub>2</sub>S-induced toxicity observed *in vivo* is the emerging role of transient receptor potential (TRP) channels as primary mediators of physiological signals mediated by low levels of this gas in several organs, including the brain (Roa-Coria et al., 2019). We therefore examined whether 2-APB, a nonselective inhibitor of TRP channels, many of which function as store operated Ca<sup>2+</sup> channels, (Baba et al., 2003) influence H<sub>2</sub>S-modified phases of SCO dysfunction described above. Mouse PCN were pretreated with 2.5–10 μM 2-APB before exposure to high concentrations of H<sub>2</sub>S mitigated the influences of H<sub>2</sub>S (Figure 5A, representative traces). 2-APB by itself at 10 μM showed a tendency to increase peak count during Phase 1, although the difference did not reach statistical significance (Figure 5Bi) until Phase 2 (Figure 5Bii). 2-APB at 10 μM antagonized H<sub>2</sub>S-induced suppression of SCO in Phases 2 and 3. Intracellular Ca<sup>2+</sup> levels were measured, and synchronous Ca<sup>2+</sup> oscillations were analyzed. Pre-exposure to 10 μM 2-APB effectively antagonized the effects of H<sub>2</sub>S in Phases 2 and 3. Pretreatment with 2-APB dose-dependently increased peak counts in Phase 2 (Figure 5Bii). Also in Phase 2, 2-APB at 10 μM significantly antagonized H<sub>2</sub>S-induced increase in peak width and peak decay time (Figs. 5Biii and 5Biv). Results in Phase 3 were like those in Phase 2 (data not shown).

To further investigate the role of endoplasmic reticulum (ER)-derived calcium in H<sub>2</sub>S-induced suppression of SCO we used dantrolene, a ryanodine receptor signaling inhibitor, as a pharmacological probe (Hayashi et al., 1997). Preliminary dose-range finding studies were done to optimize the concentration of dantrolene for use in this experiment. It is interesting that dantrolene did not show efficacy in preventing H<sub>2</sub>S-induced suppression of SCO (Figure 6A).

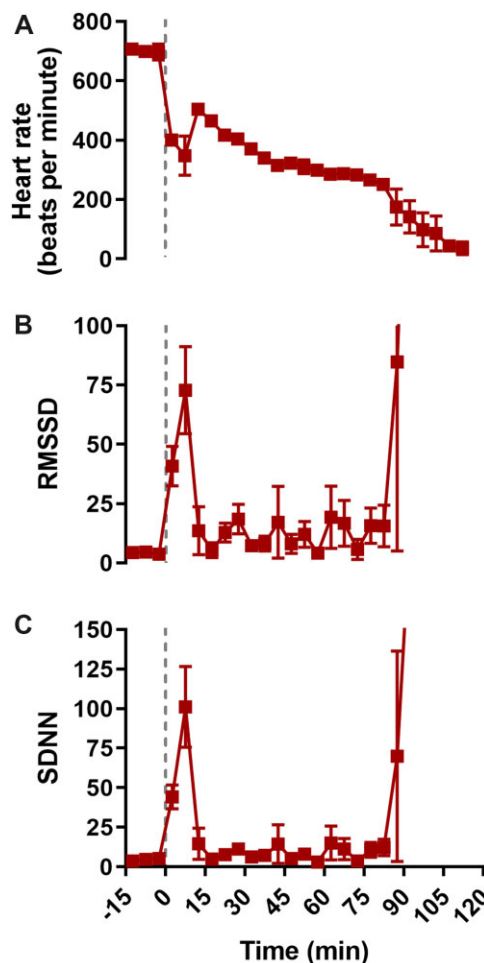


**Figure 3.** H<sub>2</sub>S exposure was characterized by an initial phase of decreased heart rate and increased heart rate variability. Time series data depicting heart rate (A, beats per minute), root-mean square differences of successive R-R intervals (B; RMSSD, ms), and standard deviations of R-R intervals (C, SDNN, ms) before and during exposure to 1000 ppm H<sub>2</sub>S. Data were depicted as mean with SEM,  $n = 3$  mice. Baseline was defined as the 15 min prior to H<sub>2</sub>S administration. Grey dotted line, start of H<sub>2</sub>S exposure. Abbreviations: H<sub>2</sub>S, hydrogen sulfide.

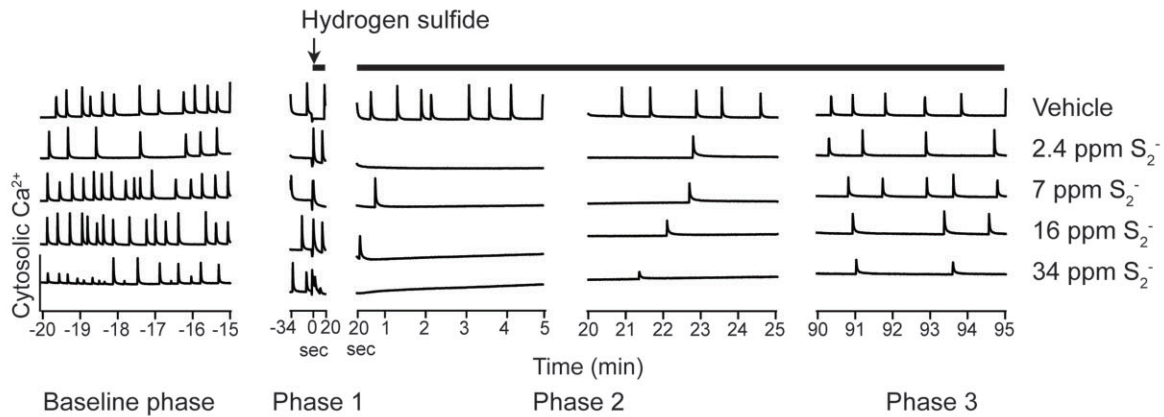
#### Ca<sup>2+</sup> channel blockers differentially influence abnormal SCO patterns triggered by H<sub>2</sub>S

We proceeded to investigate pharmacological blockers with a spectrum of selectivity toward a number of neuronal voltage-dependent Ca<sup>2+</sup> channels to determine whether the mitigating effects observed with 2-APB could be generalized. Basal SCO activities were recorded prior to application of pharmacological drugs as depicted with baseline shown in Figure 7A. PCN were pretreated with nifedipine (1–10 μM), followed by exposure to high concentration of H<sub>2</sub>S (34 ppm S<sup>2-</sup>). SCOs in each phase were assessed (Figs. 7B and 7C). Pretreatment with nifedipine significantly and dose-dependently increased acute H<sub>2</sub>S-induced SCO peak counts in Phase 1 compared to vehicle (control) group (Figure 7Bi). Although nifedipine dose-dependently reduced peak width and peak decay time in Phase 1, these were not statistically significant compared to vehicle control (Figs. 7Bii and 7Biii).

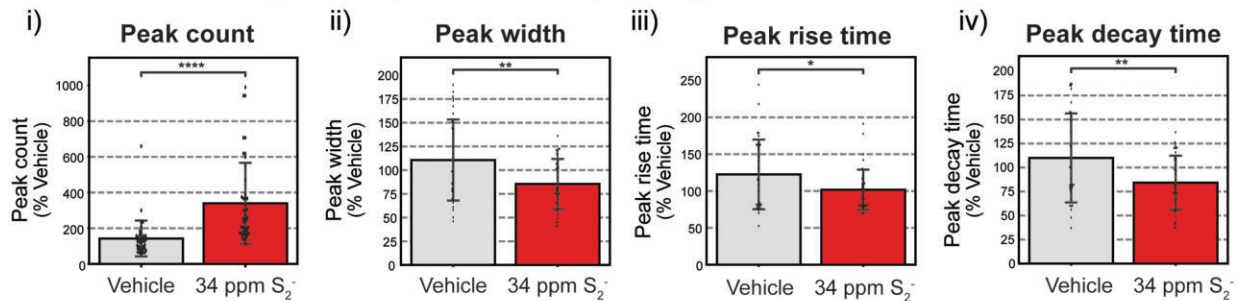
Consistent with results shown in Figure 4 H<sub>2</sub>S suppressed peak counts in Phase 2 but pretreatment with nifedipine antagonized this H<sub>2</sub>S-induced effect at 6 and 10 μM concentrations (Figure 7Ci). In Phase 2 H<sub>2</sub>S increased both peak width and peak decay time consistent with observations in Figure 4. Notably,



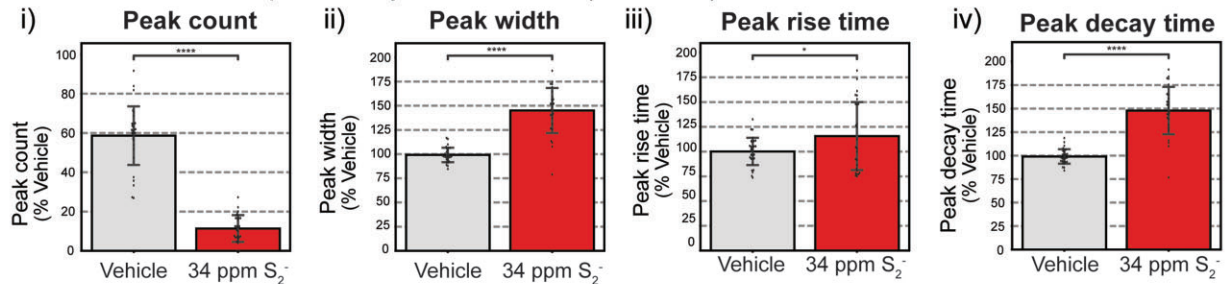
### A Ca<sup>2+</sup> oscillation peaks



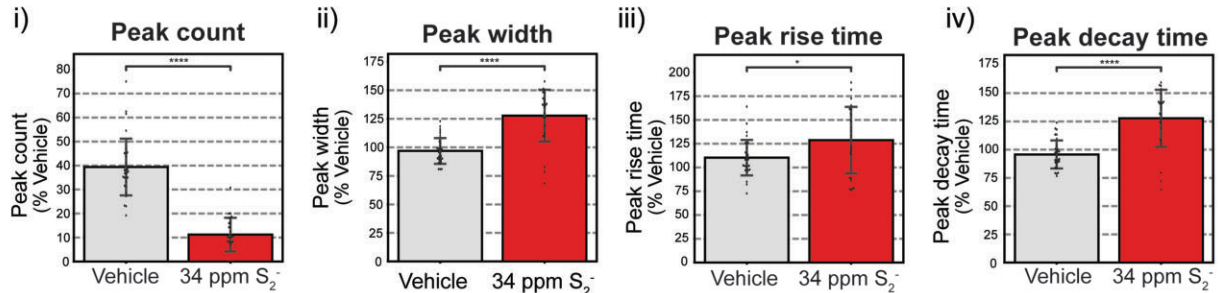
### B Ca<sup>2+</sup> oscillation peak analysis in Phase 1 (0-20sec)



### C Ca<sup>2+</sup> oscillation peak analysis in Phase 2 (20-25min)

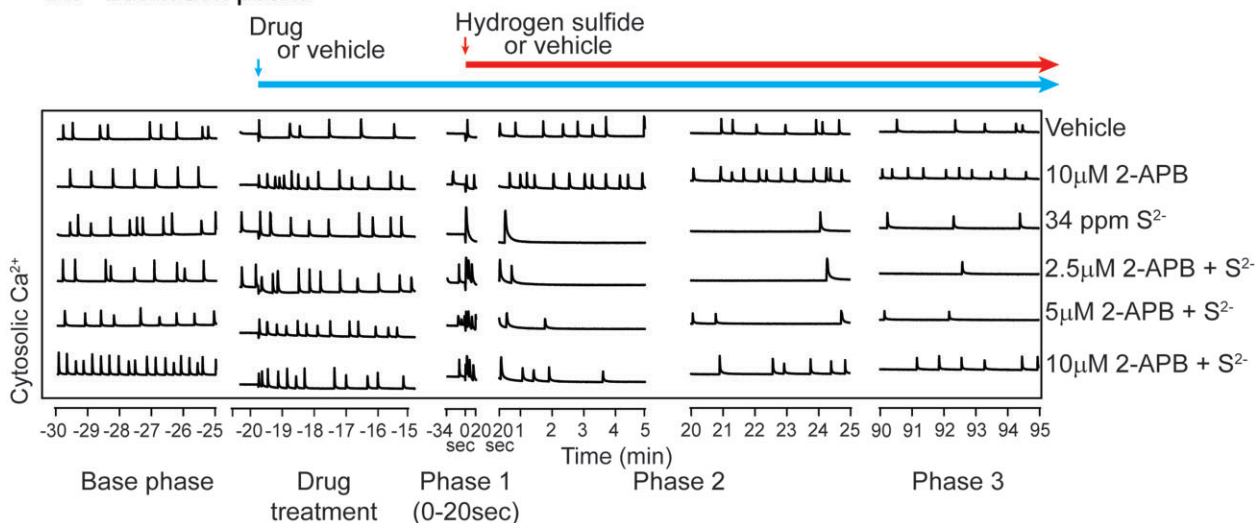
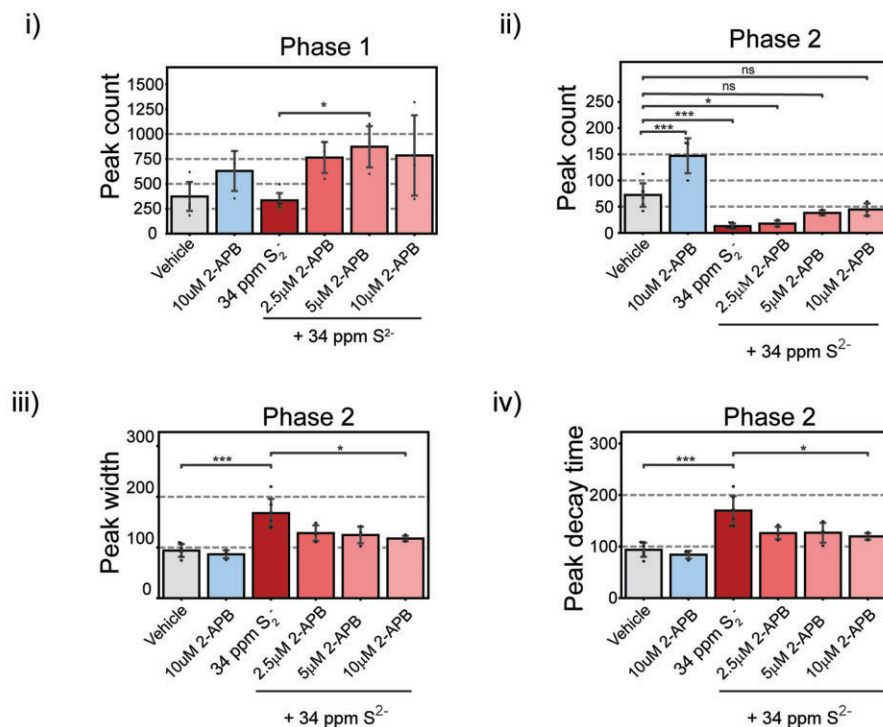


### D Ca<sup>2+</sup> oscillation peak analysis in Phase 3 (90-95min)



**Figure 4.** Synchronous calcium oscillations (SCO) in primary cortical neurons following exposure to H<sub>2</sub>S. Mouse PCN were exposed to graded concentrations of H<sub>2</sub>S. Intracellular Ca<sup>2+</sup> levels were measured, and synchronous Ca<sup>2+</sup> oscillations were analyzed. A, Traces of Ca<sup>2+</sup> oscillations to show dose-response-related effects of H<sub>2</sub>S exposure. A summary of SCO parameters in H<sub>2</sub>S exposed PCN for Phase 1 (0–20s), Phase 2 (20–25 min), and Phase 3 (90–95 min) is shown in graphs B, C, and D, respectively. Please note that H<sub>2</sub>S increased peak counts in Phase 1 but significantly suppressed this parameter in Phases 2 and 3. Also note that peak width, peak rise time, and peak decay time in Phase 1 were significantly reduced by H<sub>2</sub>S but significantly increased (reversed) in Phases 2 and 3. *N* > 30. Values are presented as mean ± standard deviation of multiple biological replicates. Each data point represents biological data from cells in a single well. This data are from more than 30 biological replicates that were pooled from 7 experiments of isolated primary cortical neurons. Student's *t* test was performed for statistical significance. Asterisks indicate significant differences compared to vehicle group. \**p* < .05, \*\**p* < .01, and \*\*\*\**p* < .0001. Abbreviations: H<sub>2</sub>S, hydrogen sulfide.



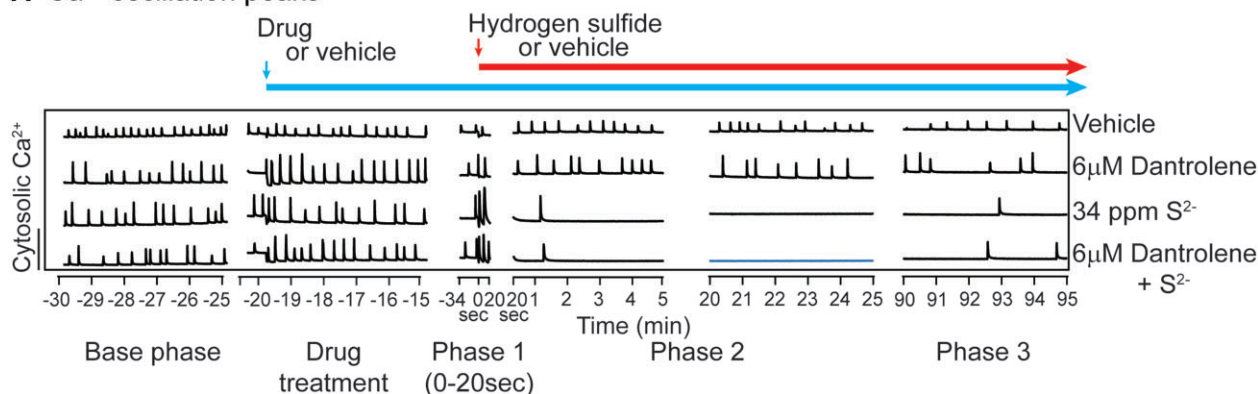
A Ca<sup>2+</sup> oscillation peaksB Ca<sup>2+</sup> oscillation peak analysis

**Figure 5.** 2-APB at 10  $\mu\text{M}$  antagonized H<sub>2</sub>S-induced suppression of SCO in Phases 2 and 3 (A). Mouse PCN were pretreated with 2.5–10  $\mu\text{M}$  2-APB before exposure to H<sub>2</sub>S. Intracellular Ca<sup>2+</sup> levels were measured, and synchronous Ca<sup>2+</sup> oscillations were analyzed. 2-APB by itself at 10  $\mu\text{M}$  significantly increased peak counts in Phase 2 (Bii). B. Analysis of SCO in H<sub>2</sub>S exposed cortical primary neurons. In Phase 2, 2-APB at 10  $\mu\text{M}$  significantly antagonized H<sub>2</sub>S-induced increase in peak width and peak decay time (Biii and Biv). Results in Phase 3 are similar to Phase 2 (data not shown).  $N = 3$ . Values are presented as mean  $\pm$  standard deviation. ANOVA with *post hoc* Tukey HSD test was performed for statistical significance. Asterisks indicate significant differences compared to vehicle group. \* $p < .05$  and \*\*\* $p < .001$ . Abbreviations: 2-APB, 2-aminoethoxydiphenylborate; H<sub>2</sub>S, hydrogen sulfide; PCN, primary cortical neuronal coculture; SCO, synchronous calcium oscillation.

pretreatment with 6 or 10  $\mu\text{M}$  nifedipine prevented H<sub>2</sub>S-induced increase in peak width (Figure 7Cii) and peak decay time (Figure 7Ciii). Effects of Nif in Phase 3 were like those in Phase 2 (data not shown). An interesting observation was that pretreatment with nimodipine, a chemically related L-type voltage-gated Ca<sup>2+</sup> channel inhibitor, failed to prevent H<sub>2</sub>S-induced suppression of SCO in PCN (Figs. 8Aiii and 8Biii).

To investigate the role T type Ca<sup>2+</sup> channels play in H<sub>2</sub>S-induced neurotoxicity, ethosuximide, a T type Ca<sup>2+</sup> channel blocker, was used. As was the case for nifedipine and nimodipine, preliminary dose-range finding studies were done to select the ideal test dose for ethosuximide, lamotrigine, and nimodipine. Pretreatment with ethosuximide did not prevent H<sub>2</sub>S-induced suppression of SCO peak counts (Figs. 8Ai and 8Bi). We then used

### A $\text{Ca}^{2+}$ oscillation peaks



### B $\text{Ca}^{2+}$ oscillation peak analysis

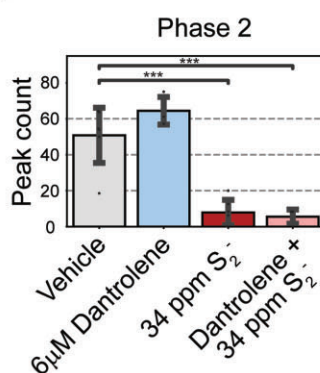


**Figure 6.** Mouse PCN were pretreated with 6  $\mu\text{M}$  dantrolene before exposure to  $\text{H}_2\text{S}$ . Intracellular  $\text{Ca}^{2+}$  levels were measured, and synchronous  $\text{Ca}^{2+}$  oscillations were analyzed. A, Traces of  $\text{Ca}^{2+}$  oscillations are shown. Note that pretreatment with dantrolene had no impact on  $\text{H}_2\text{S}$ -induced SCO in Phases 2 and 3. B, A summary of SCO peak counts in  $\text{H}_2\text{S}$  exposed cortical primary neurons in Phase 2. Note that dantrolene failed to prevent on  $\text{H}_2\text{S}$ -induced suppression of peak counts. Similar results were observed for peak width and peak decay time in Phases 2 and 3 (data not shown).  $N = 3$ . Values are presented as mean  $\pm$  standard deviation. ANOVA with *post hoc* Tukey HSD test was performed for statistical significance. Asterisks indicate significant differences compared to vehicle group. \*\*\* $p < .001$ . Abbreviations:  $\text{H}_2\text{S}$ , hydrogen sulfide; PCN, primary cortical neuronal coculture; SCO, synchronous calcium oscillation.

lamotrigine to investigate the effects of sodium channels on  $\text{H}_2\text{S}$ -induced toxicity. Lamotrigine is a voltage-dependent sodium channel blocker (Cheung et al., 1992). Pretreatment with lamotrigine also failed to antagonize the effects of  $\text{H}_2\text{S}$ -induced dysregulation on SCO in both Phase 1 and Phase 2 (Figure 8Aii).

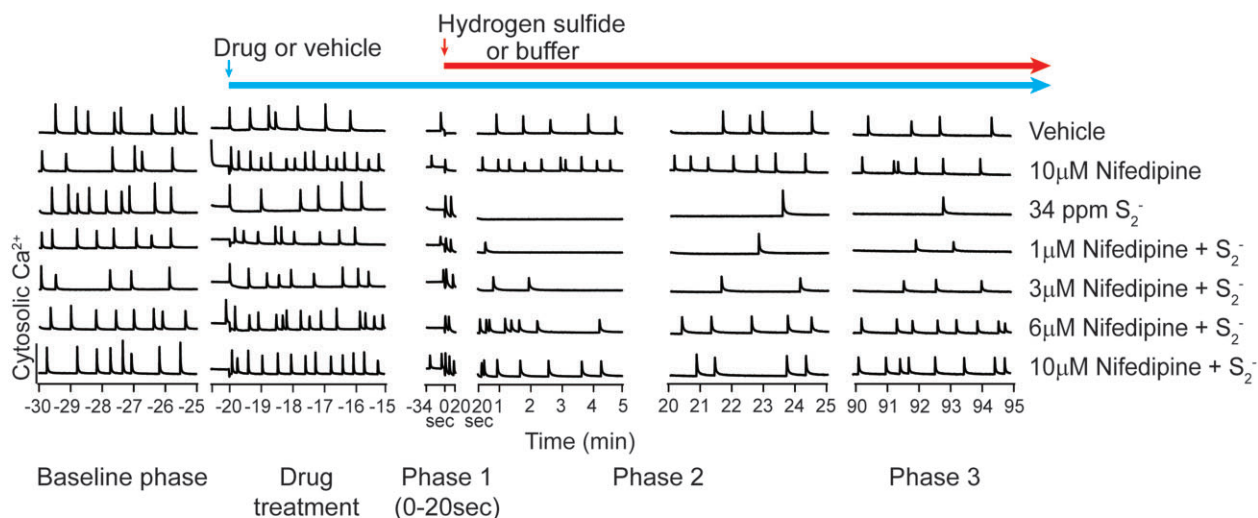
#### NMDA and AMPA receptor antagonists failed to prevent $\text{H}_2\text{S}$ -induced suppression of SCO

It has been reported that  $\text{H}_2\text{S}$  toxicity is mediated by glutamate (Cheung et al., 2007) and that it induces influx of  $\text{Ca}^{2+}$  through NMDA receptors. MK-801, an NMDA receptor inhibitor, was used to investigate the role of NMDA receptors in  $\text{H}_2\text{S}$ -induced suppression of SCO (Figure 9). As with other pharmacological probes, preliminary range finding studies were performed to select the optimal concentration for MK-801 and perampanel (an AMPA receptor blocker) (Joshi et al., 2011). Pretreatment of PCN with MK-801 alone induced suppression of SCO. Addition of high concentration of  $\text{H}_2\text{S}$  exacerbated the MK-801-induced suppression of SCO in PCN (Figs. 9Ai and 9Bii). Pretreatment of PCN with perampanel, suppressed SCO activity (Figs. 9Aii, 9Biii, and 9Biv). Unique among all drug probes used in this study, perampanel prevented  $\text{H}_2\text{S}$ -induced increase in peak counts in Phase 1 (Figure 9Biii). However, in Phase 2, pretreatment with perampanel augmented  $\text{H}_2\text{S}$ -induced suppression of SCO in PCN (Figure 9Biv).

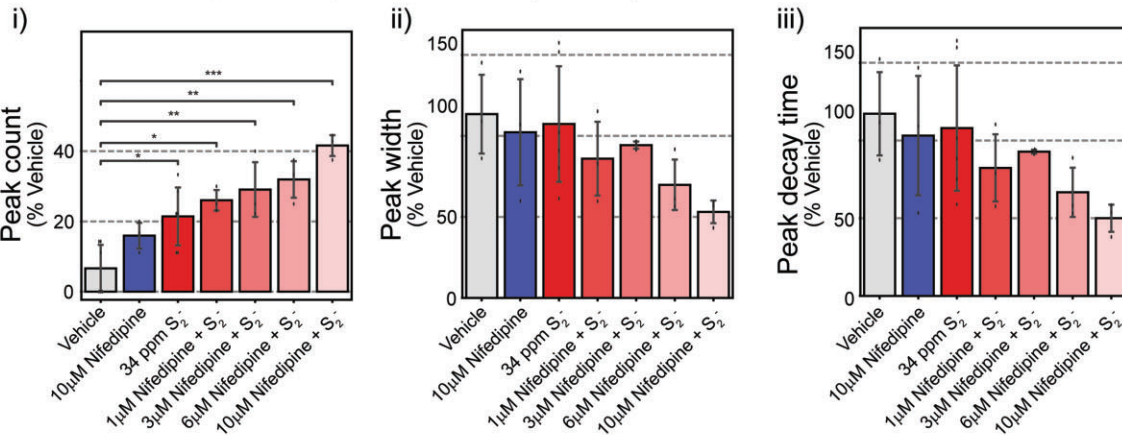
#### Pretreatment with 2-APB prevented $\text{H}_2\text{S}$ -induced suppression of neuronal electrical network spike activity in primary cortical neurons using MEA

Considering the overall activity of 2-APB toward mitigating the 3 phases of  $\text{H}_2\text{S}$ -triggered SCO dysfunction, we plated PCN on MEAs to measure electrical spike activity (Johnstone et al., 2010). Spontaneous neuronal electrical spike activity in PCN at rest was measured before treatments to obtain 10 min of baseline. Following recording of baseline activity, PCN were pretreated with 10  $\mu\text{M}$  2-APB or buffer 20 min before addition of a high concentration of  $\text{H}_2\text{S}$  (34 ppm  $\text{S}^{2-}$ ). Recording of neuronal electrical activity was initiated 1 min before  $\text{H}_2\text{S}$  was added (Figure 10A). Neuronal spike activity was detected by the Axis software. Addition of  $\text{H}_2\text{S}$  immediately induced hyperactive electrical stimulation by more than 75% compared to vehicle group (Figs. 10A and 10Bi) which was followed by suppression of electrical activity (Figs. 10A and 10Bii). We named the hyperexcitation period as Phase 1 and the suppression phase as Phase 2, similar to our data analysis strategy with FLIPR. Pretreatment with 2-APB prevented  $\text{H}_2\text{S}$ -induced acute hyper-active electrical activity in Phase 1. Whereas  $\text{H}_2\text{S}$  significantly suppressed neuronal electrical activity in Phase 2 (20 min after  $\text{H}_2\text{S}$  exposure), 2-APB pretreatment modestly prevented  $\text{H}_2\text{S}$ -induced suppression of neuronal electric activity by 27% compared to the vehicle group (Fig. 10Bii).

### A Ca<sup>2+</sup> oscillation peaks



### B Ca<sup>2+</sup> oscillation peak analysis in Phase 1 (0-20sec)



### C Ca<sup>2+</sup> oscillation peak analysis in Phase 2 (20-25min)

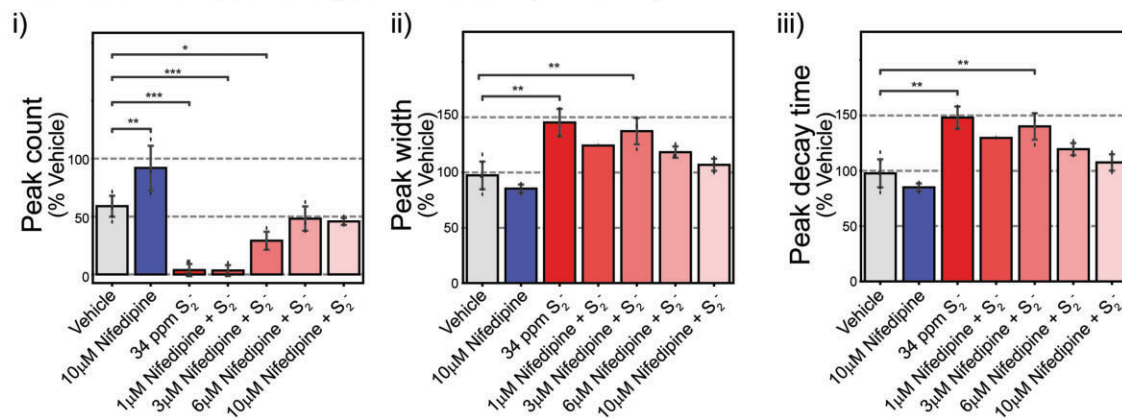
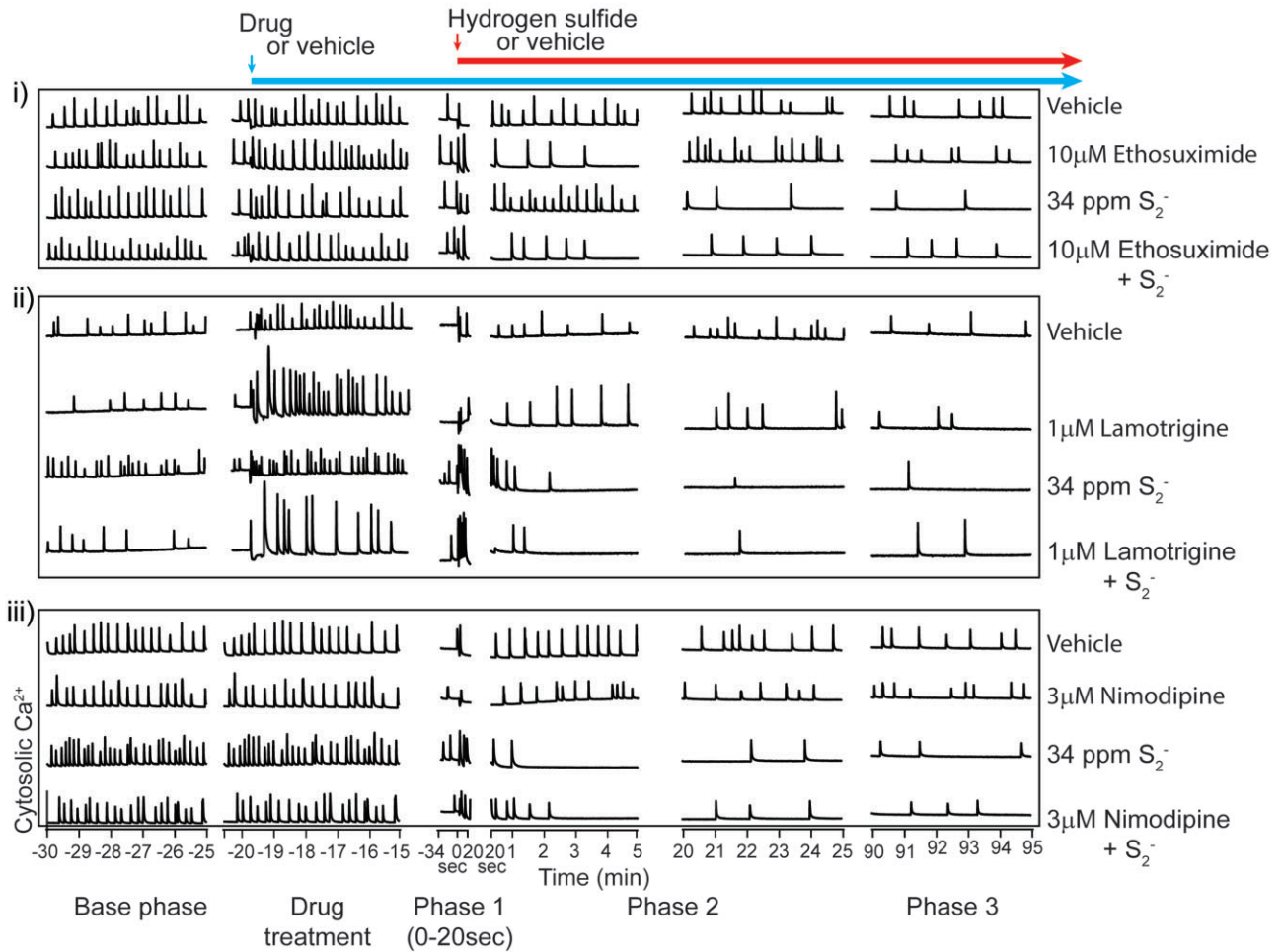


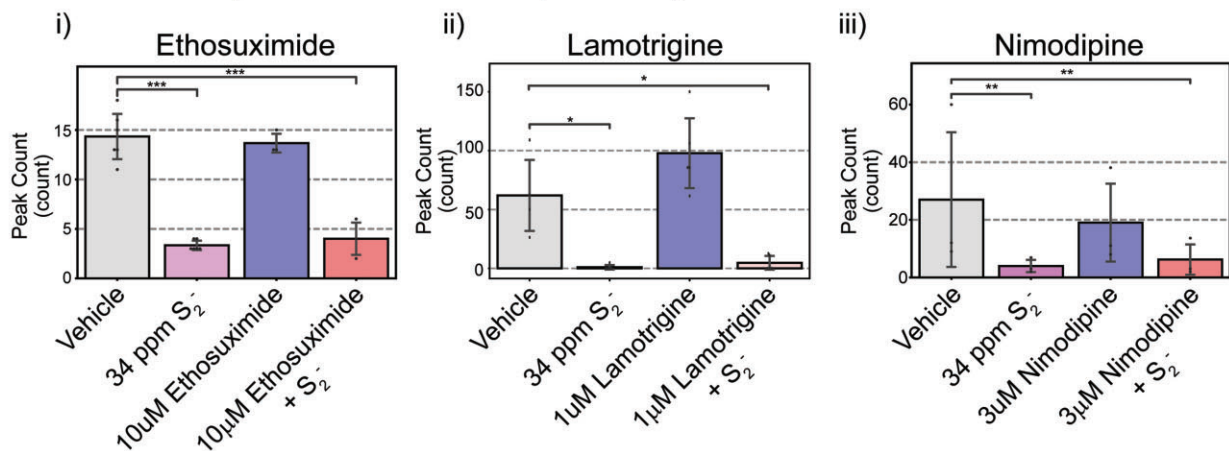
**Figure 7.** Pre-exposure to nifedipine, an inhibitor of L-type voltage-dependent calcium channel, antagonized H<sub>2</sub>S-induced suppression of SCO in Phases 1-3 at 6 and 10 μM in mouse PCN. Intracellular Ca<sup>2+</sup> levels were measured, and SCO were analyzed. A, Traces of Ca<sup>2+</sup> oscillations showing that nifedipine at 6 and 10 μM effectively prevented H<sub>2</sub>S-induced dysregulation of SCO. A summary of SCO characteristics in H<sub>2</sub>S exposed PCN for Phase 1 (0-20 s) and Phase 2 (20-25 min) in B and C. Effects of nifedipine in Phase 3 were similar to those in Phase 2 (data not shown). *N* = 3. Values are presented as mean ± standard deviation. ANOVA with *post hoc* Tukey HSD test was performed for statistical significance. Asterisks indicate significant differences compared to vehicle group. \**p* < .05, \*\**p* < .01, and \*\*\**p* < .001. Abbreviations: H<sub>2</sub>S, hydrogen sulfide; PCN, primary cortical neuronal coculture; SCO, synchronous calcium oscillation.



### A Ca<sup>2+</sup> oscillation peaks

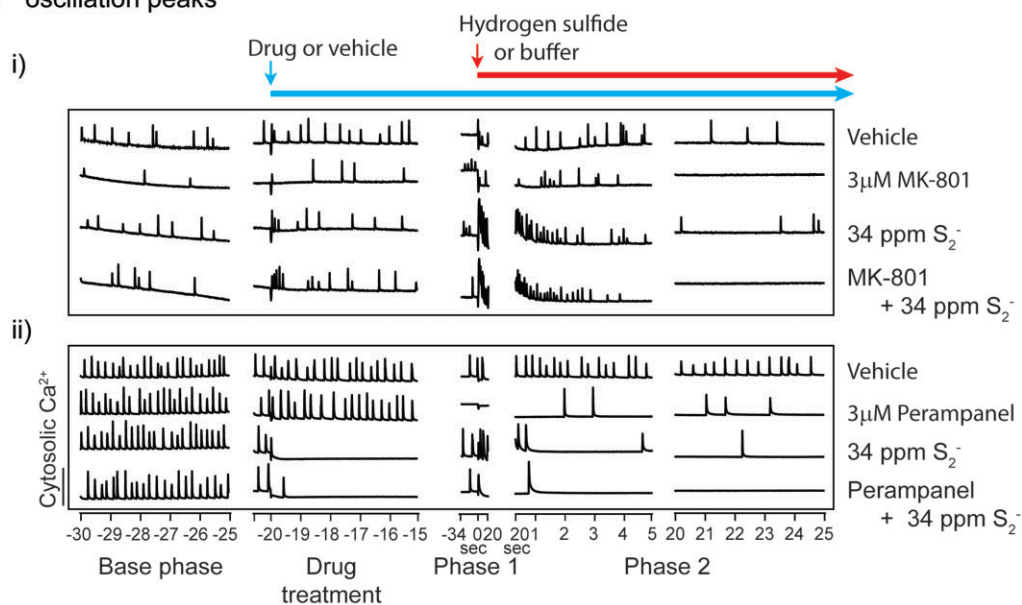
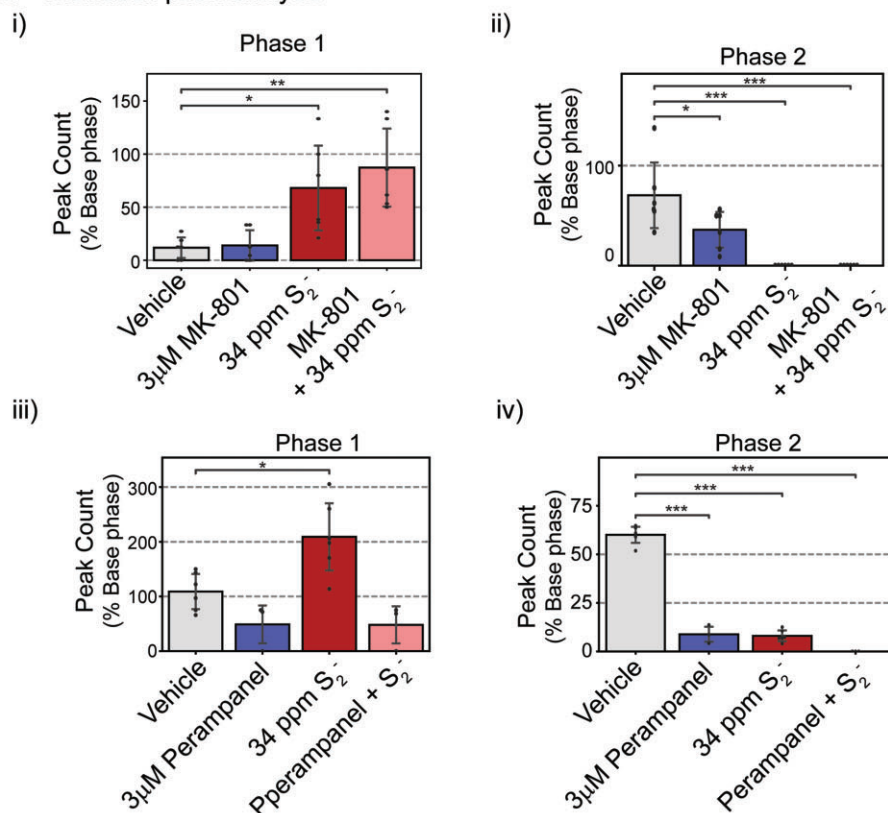


### B Ca<sup>2+</sup> oscillation peak counts in Phase 2 (20-25 min)



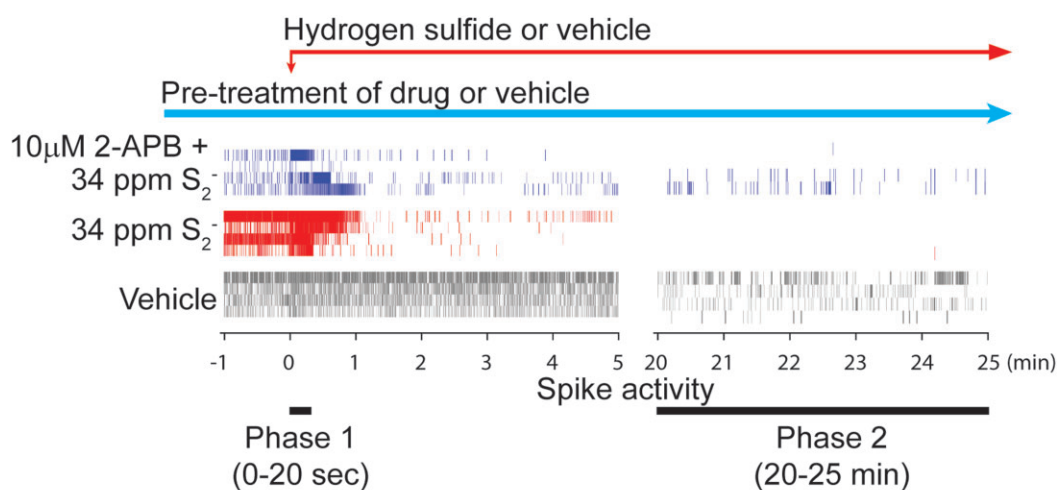
**Figure 8.** Ethosuximide, lamotrigine, and nimodipine failed to prevent H<sub>2</sub>S-induced suppression of SCO. Mouse cortical primary neurons were pretreated with ethosuximide, lamotrigine, or nimodipine before exposure to H<sub>2</sub>S. Intracellular Ca<sup>2+</sup> levels were measured, and synchronous Ca<sup>2+</sup> oscillations were analyzed. A, Traces of Ca<sup>2+</sup> oscillations. B, A summary of analyses of SCO activity in H<sub>2</sub>S exposed cortical primary neurons following pretreatment with ethosuximide, lamotrigine, and nimodipine. N = 3. Values are presented as mean ± standard deviation. ANOVA with *post hoc* Tukey HSD test was performed for statistical significance. Asterisks indicate significant differences compared to vehicle group. \**p* < .05, \*\**p* < .01, and \*\*\**p* < .001. Abbreviations: H<sub>2</sub>S, hydrogen sulfide; SCO, synchronous calcium oscillation.



**A Ca<sup>2+</sup> oscillation peaks****B Ca<sup>2+</sup> oscillation peak analysis**

**Figure 9.** Mouse PCN were pretreated with MK-801 or perampanel before exposure to H<sub>2</sub>S. Intracellular Ca<sup>2+</sup> levels were measured, and synchronous Ca<sup>2+</sup> oscillations were analyzed. A, Traces of Ca<sup>2+</sup> oscillations were shown. Inhibitors for NMDA receptor and AMPA receptor failed to antagonize H<sub>2</sub>S-induced suppression of SCO in Phase 2 (A). B, Analysis of SCO in H<sub>2</sub>S exposed PCN. MK-801 failed to prevent H<sub>2</sub>S-induced effects on peak counts in Phases 1 and 2 (Bi and Bii). Perampanel significantly prevented H<sub>2</sub>S-induced increase in peak counts in Phase 1 (Biii) but worsened H<sub>2</sub>S-induced decrease in peak counts in Phase 2 (Biv). N = 3. Values are presented as mean ± standard deviation. ANOVA with *post hoc* Tukey HSD test was performed for statistical significance. Asterisks indicate significant differences compared to vehicle group. \**p* < .05 and \*\*\**p* < .001. Abbreviations: H<sub>2</sub>S, hydrogen sulfide; PCN, primary cortical neuronal coculture; SCO, synchronous calcium oscillation.

## A Spontaneous electrical spike activity



## B Quantification of spontaneous electrical spike activity

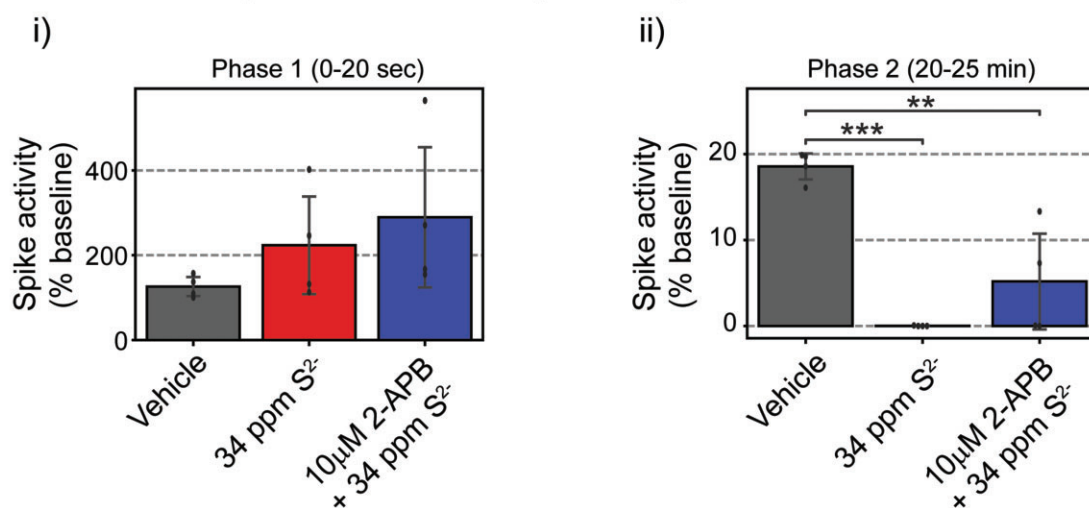


**Figure 10.** Neuronal electrical activities were measured using the multiple-electrode array system (MEA). Mouse PCN were pretreated with 2-APB or vehicle before exposure to a H<sub>2</sub>S donor. A, spontaneous neuronal electrical spike activities are shown. Addition of H<sub>2</sub>S-induced hyperactive electrical spike activity in Phase 1, whereas pretreatment with 2-APB modestly antagonized H<sub>2</sub>S-induced suppression of electrical activity in Phases 1 and 2. B, Spontaneous electrical spike activities in PCN were quantified. Note that pretreatment with 2-APB modestly antagonized H<sub>2</sub>S-induced suppression of electrical activity in Phase 2 (Bii). N = 4. Values are presented as mean ± standard deviation. ANOVA with post hoc Tukey HSD test was performed for statistical significance. Asterisks indicate significant differences compared to vehicle group. \*\*p < .01 and \*\*\*p < .001. Abbreviations: 2-APB, 2-aminoethoxydiphenylborate; H<sub>2</sub>S, hydrogen sulfide; PCN, primary cortical neuronal coculture.

### 2-APB protected cortical neurons from H<sub>2</sub>S-induced cell death

Of the diverse ion channel probes investigated in this study, 2-APB was the most interesting as far as antagonizing effects of H<sub>2</sub>S on SCO. We therefore investigated whether the antagonistic effects of 2-APB observed in this study had impact on H<sub>2</sub>S-induced neuronal cell death. To do this, a cell viability assay was performed using ImageXpress<sup>®</sup> Micro (Molecular Devices) and cell-permeant dye, calcein AM, according to the manufacturer's protocol (Figure 11). PCN DIV 9–15 were pretreated with 2-APB or buffer 10 min before exposure to a high concentration of H<sub>2</sub>S (34 ppm S<sub>2</sub><sup>-</sup>) for 40 min. The H<sub>2</sub>S exposure medium was then replaced with fresh cell growing medium. Cells were incubated for 72 h after H<sub>2</sub>S exposure before assessing cell death by

counting the live cells using fluorescent calcein dye (Figure 11A). A summary of results of live cells is shown in Figure 11B. H<sub>2</sub>S by itself induced about 50% cell mortality. For cells pretreated with 10 µM 2-APB, only 25% cell mortality was observed (Figure 11B). These preliminary results suggest that 2-APB was neuroprotective in this model.

## Discussion

The toxicity of H<sub>2</sub>S is complex and the proximate cause of death following acute high concentrations of H<sub>2</sub>S exposure is debatable. Moreover, the molecular mechanisms of H<sub>2</sub>S-induced neurotoxicity are not known. The study addressed several of these gaps in knowledge. First, in the *in vivo* study we show that it is

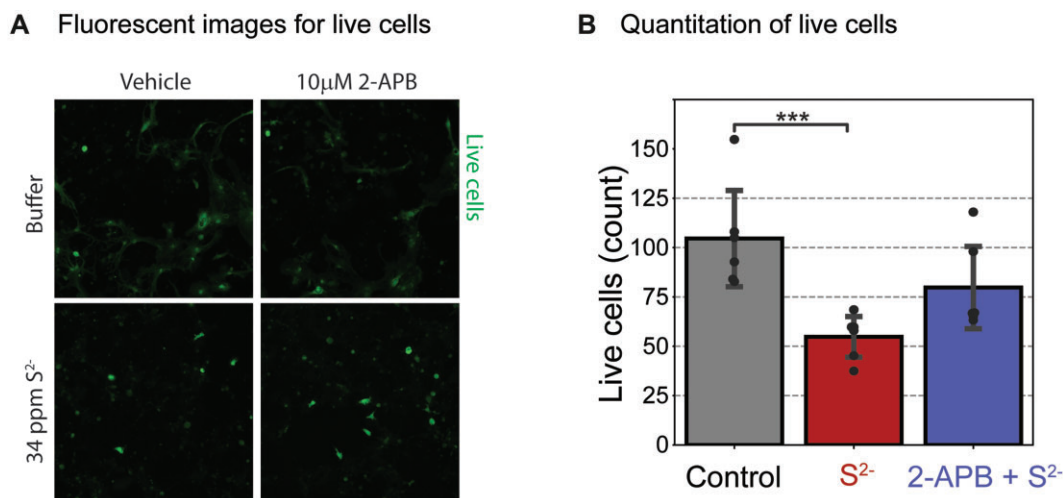


**Figure 11.** Mouse PCN were pretreated with 10 µM 2-APB and exposed to H<sub>2</sub>S for 40 min only. The cells were washed and incubated for 72 h before imaging of live cells to assess cell survival. A, Live cortical neurons were imaged using cell-permeable calcein AM fluorescent dye. B, A summary of results. Pretreatment with 2-APB significantly increased cell survival compared to the H<sub>2</sub>S group. N = 6. Values are presented as mean ± standard deviation. ANOVA with post hoc Tukey HSD test was performed for statistical significance. Asterisks indicate significant differences compared to Control group. \*\*\*p < .001. Abbreviations: 2-APB, 2-aminoethoxydiphenylborate; H<sub>2</sub>S, hydrogen sulfide; PCN, primary cortical neuronal coculture.

electrocerebral suppression which precipitates respiratory suppression and outright apnea. Cardiac arrest is of later onset and likely a consequence of hypoxia due to prolonged respiratory insufficiency and/or H<sub>2</sub>S-induced lack of ATP. The onset of H<sub>2</sub>S exposure mildly decreased cardiac activity and increased heart rate variability. These mild changes in heart function partially recovered early during exposure. In contrast, respiratory suppression was severe and did not recover (Figs. 2 and 3). H<sub>2</sub>S exposure rapidly elicited a burst-suppressed EEG pattern in which periods of electrographic suppression frequently coincided with apnea (Figure 1). As the exposure progressed, periods of bursting became less regular giving way to complete electrocerebral suppression (Figure 1). This progressive electrocerebral dysfunction was temporally mirrored by progressive decreases in breathing until respiration was no longer compatible with life (Figs. 1 and 3). It is interesting however that we did not see clear epileptiform discharges in this study, suggesting that the electrographic seizure activity was localized to the brainstem. This is supported by our observations that seizure activity in this model are akin to audiogenic induced seizures in DBA mice and other models which originate from the brainstem.

Respiratory rhythmogenesis is a function of the brain, specifically pre-Bötzing complex within the ventrolateral medulla (Smith et al., 1991). The coincidence between episodes of electrocerebral suppression and frank apnea may be indicative of transient periods neuronal inactivity across the entirety of the brain, including the respiratory nuclei of the brainstem. The data presented here indicate that (1) the electrocerebral dysfunction induced by H<sub>2</sub>S exposure is the driving force behind the respiratory dysfunction and (2) the cardiac dysfunction observed in the later stages of H<sub>2</sub>S exposure are causally downstream to the electrocerebral/respiratory dysfunction.

To further understand the mechanisms involved in electrocerebral suppression, we developed an *in vitro* model of PCN which recapitulated the *in vivo* H<sub>2</sub>S-induced EEG using SCO in FLIPR and electrical spike activity using MEA. In this study we used PCN because primary neuron/astrocyte coculture have functional receptors, unlike immortalized cell lines. FLIPR is a

fluorescent plate reader-based assays that allows fast and simultaneous readings of intracellular Ca<sup>2+</sup> of cells in multiple wells. Use of PCN with rapid-throughput systems using FLIPR and MEA allowed us to gain insights in the role of the various calcium channels in acute H<sub>2</sub>S-induced toxicity on the brain.

SCO is driven by action potentials in the neurons. The infinite patterns of frequency of SCO and changes of SCO frequency or amplitude provides important means to fulfill diverse cellular and tissue functions (Smedler and Uhlen, 2014). Dysregulation of SCO in neurons is also implicated in toxicant-induced neuronal dysfunction (Cao et al., 2012). As shown in FLIPR experiments, H<sub>2</sub>S induced an acute hyper-active neuronal firing upon addition of H<sub>2</sub>S (Phase 1), followed by suppression of spontaneous neuronal firings in MEA system (Phase 2). The acute hyper-active SCO and neuronal firing is akin to the seizure like burst suppression activity that was observed *in vivo* whereas suppressed SCO and suppressed neuronal firings are akin to loss of consciousness or central nervous system depression characteristic of acute H<sub>2</sub>S poisoning.

Acute hyper-active SCO in Phase 1 was characterized by increased SCO peak count and a shorter SCO peak rise time, width, and decay time indicating the cycle of SCO is much faster, which is also corresponds with the acute hyper-active neuronal firings in the MEA system. Phase 2 SCO is characterized by wider peak width and by increased SCO peak decay time. Action potential drives SCO in cortical neurons (Robinson et al., 1993), and action potential initiates opening of sodium channels in neurons (Grider et al., 2022). We hypothesize that the acute hyper-active SCO plays a role in prolonged suppression of SCO in PCN. Treatment with 1 µM lamotrigine, a sodium channel blocker, by itself significantly decreased SCO peak count in Phase 1, whereas 30 µM lamotrigine completely abolished SCO in Phase 1 (data not shown). However, lamotrigine failed to prevent H<sub>2</sub>S-induced acute hyper-active SCO in Phase 1, within 20 s of adding H<sub>2</sub>S (data not shown). These results indicate that H<sub>2</sub>S may induce acute hyper excitability in neurons in Phase 1 via a different mechanism other than through the lamotrigine-sensitive sodium channel.

Neurons have numerous  $\text{Ca}^{2+}$  channels targeted to specific anatomical regions that mediate specific physiological functions (Berridge, 2016; Brini et al., 2014). We investigated select  $\text{Ca}^{2+}$  channel blockers for their ability to reverse  $\text{H}_2\text{S}$ -induced dysregulation of SCO including acute hyper-active (Phase 1), prolonged suppression (Phase 2) and recovery (Phase 3) SCO epochs that we identified as biomarkers of cellular dysfunction using the FLIPR Tetra<sup>®</sup> imaging system. We observed that not all  $\text{Ca}^{2+}$  channel blockers had the same influence on the 3 phases of  $\text{H}_2\text{S}$ -triggered  $\text{Ca}^{2+}$  dysregulation. Moreover, those that showed efficacy toward antagonizing effects of  $\text{H}_2\text{S}$  did not reverse all 3 phases of dysfunction. For example, nifedipine failed to suppress acute hyper-active SCO in Phase 1 but it reversed  $\text{H}_2\text{S}$ -induced suppression of SCO in Phase 2. It is not clear what the exact mechanism(s) behind nifedipine-induced reversal of suppressed SCO by  $\text{H}_2\text{S}$  exposure are at this time. Further research is needed to understand more about nifedipine-induced reversal of SCO when PCN culture was exposed to  $\text{H}_2\text{S}$ . Although both nifedipine and nimodipine are L type VGCC inhibitors and are used for anti-seizure treatment, they showed different efficacy toward seizures (Grabowski and Johansson, 1985; Konrad-Dalhoff et al., 1991). Nimodipine has a higher efficacy toward blocking  $\text{Ca}_v1.3_{\alpha1}$  (Xu and Lipscombe, 2001), whereas nifedipine blocks  $\text{Ca}_v1.2$  at lower concentrations than nimodipine (Wang et al., 2018). Nifedipine and nimodipine were also shown to inhibit T-type calcium channels. However, ethosuximide, another T-type calcium channel inhibitor, in this study failed to reverse  $\text{H}_2\text{S}$ -induced suppression of SCO in PCN. These results showed that  $\text{H}_2\text{S}$ -induced neurotoxicity is not mediated through T-type receptors as blockage of T-type VGCC channels using ethosuximide failed to reverse  $\text{H}_2\text{S}$ -suppressed SCO in PCN. Even though nifedipine showed efficacy in reversing  $\text{H}_2\text{S}$ -induced suppression of SCO *in vitro*, this drug was reported to induce hypotension *in vivo*.  $\text{H}_2\text{S}$  poisoning was also reported to induce hypotension (Baldelli et al., 1993) limiting the possible use of nifedipine as a drug for treating victims of  $\text{H}_2\text{S}$  poisoning.

TRP channels mediate Store-operated  $\text{Ca}^{2+}$  (SOC) entry (Lopez et al., 2020) and have previously been implicated in  $\text{H}_2\text{S}$ -induced pathophysiology (Ng et al., 2019; Pozsgai et al., 2019). Pre-exposure to 2-APB showed partial efficacy by preventing  $\text{H}_2\text{S}$ -induced suppression of SOC in Phase 2. 2-APB, like nifedipine, failed to antagonize effects of  $\text{H}_2\text{S}$  in Phase 1. Previously, SCO was shown to require cyclic  $\text{Ca}^{2+}$  entry through the NMDA receptor in cerebellar neurons via activated P-type  $\text{Ca}^{2+}$  channel (Nunez et al., 1996). We have shown that  $\text{H}_2\text{S}$  suppresses neuronal electrical activity in PCN, and that 10  $\mu\text{M}$  2-APB antagonized this, reversing it to a degree. TRP channels are a large group of channels with multiple sub-families, and diverse groups of proteins are involved (Samanta et al., 2018). 2-APB is a nonselective blocker of TRP channels and SOCE. 2-APB also antagonizes  $\text{IP}_3\text{R}$  and store-operated  $\text{Ca}^{2+}$  channel in ER (Spletstoeser et al., 2007). Activation of SOC entry is triggered by the depletion of  $\text{Ca}^{2+}$  stores in ER (Bollimuntha et al., 2017). Dantrolene antagonizes ryanodine receptor in ER and inhibits calcium release. 2-APB may also play a role in inhibiting voltage-gated and calcium-dependent potassium conductance and affecting on depolarization of membrane potential (Hagenston et al., 2009). Though promising, as a nonselective TRP blocker, 2-APB might induce off-target effects. More research is warranted to investigate the efficacy of 2-APB and to study the efficacy of other more selective TRP antagonists in acute  $\text{H}_2\text{S}$ -induced neurotoxicity.

Hydrogen sulfide is known to inhibit cytochrome c oxidase activity in mitochondria (Anantharam et al., 2017a) depleting ATP. It is plausible that  $\text{H}_2\text{S}$ -induced depletion of ATP might lead

to  $\text{Ca}^{2+}$  dysregulation via glutamate receptor. The NMDA receptor has been implicated in  $\text{H}_2\text{S}$ -induced neurotoxicity because MK-801, an NMDA receptor inhibitor protects cerebellar granule neurons (Cheung et al., 2007; Garcia-Bereguain et al., 2008). However, other investigators reported that  $\text{H}_2\text{S}$ -induced neurotoxicity was not improved by use of NMDA receptor inhibitors (Kurokawa et al., 2011). In this study, MK-801 exacerbated  $\text{H}_2\text{S}$ -induced suppression of SCO in PCN. This implies that  $\text{H}_2\text{S}$  acting through NMDA receptors plays a role in regulating SCO in PCN through  $\text{Ca}^{2+}$  signaling. Pretreatment with peramppanel also exacerbated  $\text{H}_2\text{S}$ -induced suppression of SCO. Dravid and Murray (2004) showed that glutamate and AMPA receptors play a role in spontaneous SCO in neocortical neurons. Findings from this study are consistent with those observations and is further evidence that glutamate and AMPA receptors are involved in regulating SCO during  $\text{H}_2\text{S}$  intoxication.

Hydrogen sulfide exposure induces many neurological dysfunctions including motor, behavioral, memory, and visual impairment, and induces neurological sequelae (Nam et al., 2004; Tvedt et al., 1991a) including neuronal cell death in select brain regions (Anantharam et al., 2017a,b, 2018; Kim et al., 2018, 2019). Inhibition of the breathing center in the brainstem and/or prolonged coma have been linked to death and neurological complications (Guidotti, 1994; Sonobe and Haouzi, 2015). Whether the distribution or physiological differences of calcium channels are responsible for this selective sensitivity of specific brain regions deserves investigations in future studies. In summary preventing or reversing dysregulation of  $\text{Ca}^{2+}$  signaling may be one of the ways to treat acute  $\text{H}_2\text{S}$ -induced neurotoxicity, and reduce mortality and morbidity.

## Conclusion

Hydrogen sulfide is a potent toxicant targeting the brain, lung, and heart. In this study, we examined brain, lung, and heart function in real-time during  $\text{H}_2\text{S}$  exposure.  $\text{H}_2\text{S}$  suppressed electrocerebral activity and disrupted breathing. Cardiac activity was comparatively less affected. This *in vivo* study provided direct evidence that it is the  $\text{H}_2\text{S}$ -induced dysregulation of brain activity that triggers breathing challenges and not vice versa. It also showed that heart function is the last to fail of the 3 major target organs of  $\text{H}_2\text{S}$  poisoning. We were also able to recapitulate the *in vivo* brain electrical activity using a simple *in vitro* model of PCN in 2 neuronal function assays FLIPR and MEA. Using the *in vitro* functional PCN model we showed that following a single acute  $\text{H}_2\text{S}$  exposure, 3 phases of  $\text{H}_2\text{S}$ -induced neurotoxicity were discernible using FLIPR and MEA. Phase 1 is characterized by hyperactivity. Phase 2 is characterized by suppressed electrical activity. Phase 3 is characterized by recovery.  $\text{H}_2\text{S}$  consistently induced phase-specific changes in peak count, peak width, peak rise time, and peak decay time. Using these parameters, we showed that nifedipine, an L-type voltage-gated calcium channel inhibitor antagonized  $\text{H}_2\text{S}$ -induced suppression of SCO in PCN. Surprisingly, nimodipine, another L-type voltage-gated calcium channel antagonist, failed. Blockage of Store-operated  $\text{Ca}^{2+}$  entry by 2-APB also prevented  $\text{H}_2\text{S}$ -induced suppression of SCO and neuronal electrical activity and was protective of the PCN. NMDA and AMPA receptors were shown to be involved in  $\text{H}_2\text{S}$ -induced regulation of SCO. For example, pretreatment with peramppanel effectively antagonized effects of  $\text{H}_2\text{S}$  in Phase 1. However, like MK-801, it worsened the effects of  $\text{H}_2\text{S}$  in Phase 2, further suppressing SCO. Notably, we have developed a rapid *in vitro* system consisting of FLIPR and MEA to study the role of various  $\text{Ca}^{2+}$



channels in H<sub>2</sub>S-induced neurotoxicity. Used in conjunction with ImagerExpress<sup>®</sup> high content imaging, we can also assess the neuroprotective efficacy of test articles and drug candidates to treat acute H<sub>2</sub>S-induced neurotoxicity. Drugs that can normalize H<sub>2</sub>S-induced Ca<sup>2+</sup> dysregulation may have therapeutic potential in reducing H<sub>2</sub>S-induced mortality and morbidity. We plan to use this *in vitro* system to further understand the role of calcium in H<sub>2</sub>S-induced neurotoxicity and for potential discovery of novel and repurposed drugs for treatment of acute H<sub>2</sub>S poisoning to reduce mortality and/or morbidity.

## Supplementary data

Supplementary data are available at *Toxicological Sciences* online.

## Acknowledgments

We appreciate Dr Michael A. Rogawski for generously donating the ethosuximide and perampanel for this study. We also appreciate Raissa Raineri for valuable technical support. We also acknowledge funding from Mind Institute IDDRRC (P50HD103526) for high content imaging included in this manuscript.

## Funding

Internal grants of UC Davis and Iowa State University for Wilson Rumbleiha.

## Declaration of conflicting interests

The authors declared no potential conflicts of interest with respect to the research, authorship, and/or publication of this article.

## References

- Alford, S. T., and Alpert, M. H. (2014). A synaptic mechanism for network synchrony. *Front. Cell. Neurosci.* **8**, 290.
- Anantharam, P., Kim, D. S., Whitley, E. M., Mahama, B., Imerman, P., Padhi, P., and Rumbleiha, W. K. (2018). Midazolam efficacy against acute hydrogen sulfide-induced mortality and neurotoxicity. *J. Med. Toxicol.* **14**, 79–90.
- Anantharam, P., Whitley, E. M., Mahama, B., Kim, D. S., Imerman, P. M., Shao, D., Langley, M. R., Kanthasamy, A., and Rumbleiha, W. K. (2017a). Characterizing a mouse model for evaluation of countermeasures against hydrogen sulfide-induced neurotoxicity and neurological sequelae. *Ann. N. Y. Acad. Sci.* **1400**, 46–64.
- Anantharam, P., Whitley, E. M., Mahama, B., Kim, D. S., Sarkar, S., Santana, C., Chan, A., Kanthasamy, A. G., Kanthasamy, A., Boss, G. R., et al. (2017b). Cobinamide is effective for treatment of hydrogen sulfide-induced neurological sequelae in a mouse model. *Ann. N. Y. Acad. Sci.* **1408**, 61–78.
- Baba, A., Yasui, T., Fujisawa, S., Yamada, R. X., Yamada, M. K., Nishiyama, N., Matsuki, N., and Ikegaya, Y. (2003). Activity-evoked capacitative Ca<sup>2+</sup> entry: Implications in synaptic plasticity. *J. Neurosci.* **23**, 7737–7741.
- Baldelli, R. J., Green, F. H., and Auer, R. N. (1993). Sulfide toxicity: Mechanical ventilation and hypotension determine survival rate and brain necrosis. *J. Appl. Physiol.* (1985) **75**, 1348–1353.
- Berridge, M. J. (2016). The inositol trisphosphate/calcium signaling pathway in health and disease. *Physiol. Rev.* **96**, 1261–1296.
- Binder, M. K., Quigley, J. M., and Tinsley, H. F. (2018). Islamic state chemical weapons: A case contained by its context? *CTC Sentinel* **11**, 27–31.
- Bollimuntha, S., Pani, B., and Singh, B. B. (2017). Neurological and motor disorders: Neuronal store-operated Ca(2+) signaling: An overview and its function. *Adv. Exp. Med. Biol.* **993**, 535–556.
- Brini, M., Cali, T., Ottolini, D., and Carafoli, E. (2014). Neuronal calcium signaling: Function and dysfunction. *Cell. Mol. Life Sci.* **71**, 2787–2814.
- Cao, Z., Cui, Y., Nguyen, H. M., Jenkins, D. P., Wulff, H., and Pessah, I. N. (2014). Nanomolar bifenthrin alters synchronous Ca<sup>2+</sup> oscillations and cortical neuron development independent of sodium channel activity. *Mol. Pharmacol.* **85**, 630–639.
- Cao, Z., Hammock, B. D., McCoy, M., Rogawski, M. A., Lein, P. J., and Pessah, I. N. (2012). Tetramethylenedisulfotetramine alters Ca<sup>2+</sup> dynamics in cultured hippocampal neurons: Mitigation by NMDA receptor blockade and GABA<sub>A</sub> receptor-positive modulation. *Toxicol. Sci.* **130**, 362–372.
- Cao, Z., Xu, J., Hulsizer, S., Cui, Y., Dong, Y., and Pessah, I. N. (2017). Influence of tetramethylenedisulfotetramine on synchronous calcium oscillations at distinct developmental stages of hippocampal neuronal cultures. *Neurotoxicology* **58**, 11–22.
- Cavieres-Lepe, J., and Ewer, J. (2021). Reciprocal relationship between calcium signaling and circadian clocks: Implications for calcium homeostasis, clock function, and therapeutics. *Front. Mol. Neurosci.* **14**, 666673.
- Cheung, H., Kamp, D., and Harris, E. (1992). An *in vitro* investigation of the action of lamotrigine on neuronal voltage-activated sodium channels. *Epilepsy Res.* **13**, 107–112.
- Cheung, N. S., Peng, Z. F., Chen, M. J., Moore, P. K., and Whiteman, M. (2007). Hydrogen sulfide induced neuronal death occurs via glutamate receptor and is associated with calpain activation and lysosomal rupture in mouse primary cortical neurons. *Neuropharmacology* **53**, 505–514.
- Dravid, S. M., and Murray, T. F. (2004). Spontaneous synchronized calcium oscillations in neocortical neurons in the presence of physiological [mg(2+)]: Involvement of AMPA/kainate and metabotropic glutamate receptors. *Brain Res.* **1006**, 8–17.
- Garcia-Bereguian, M. A., Samhan-Arias, A. K., Martin-Romero, F. J., and Gutierrez-Merino, C. (2008). Hydrogen sulfide raises cytosolic calcium in neurons through activation of L-type Ca<sup>2+</sup> channels. *Antioxid. Redox Signal.* **10**, 31–42.
- Glaser, T., Shimojo, H., Ribeiro, D. E., Martins, P. P. L., Beco, R. P., Kosinski, M., Sampaio, V. F. A., Correa-Velloso, J., Oliveira-Giacomelli, A., Lameu, C., et al. (2021). Atp and spontaneous calcium oscillations control neural stem cell fate determination in Huntington's disease: A novel approach for cell clock research. *Mol. Psychiatry* **26**, 2633–2650.
- Grabowski, M., and Johansson, B. B. (1985). Nifedipine and nimodipine: Effect on blood pressure and regional cerebral blood flow in conscious normotensive and hypertensive rats. *J. Cardiovasc. Pharmacol.* **7**, 1127–1133.
- Grider, M. H., Jessu, R., and Kabir, R. (2022). Physiology, action potential. In *StatPearls*. StatPearls Publishing, Treasure Island, FL.
- Grudt, T. J., Usowicz, M. M., and Henderson, G. (1996). Ca<sup>2+</sup> entry following store depletion in sh-sy5y neuroblastoma cells. *Brain Res. Mol. Brain Res.* **36**, 93–100.
- Guidotti, T. L. (1994). Occupational exposure to hydrogen sulfide in the sour gas industry: Some unresolved issues. *Int. Arch. Occup. Environ. Health* **66**, 153–160.
- Guidotti, T. L. (2010). Hydrogen sulfide: Advances in understanding human toxicity. *Int. J. Toxicol.* **29**, 569–581.

- Guidotti, T. L. (2015). Hydrogen sulfide intoxication. In *Handbook of Clinical Neurology* (M. Lotti and M. L. Bleeker, Eds.), 3rd ed., Vol. 131, pp. 111–133. Elsevier, Cambridge, MA.
- Hagenston, A. M., Rudnick, N. D., Boone, C. E., and Yeckel, M. F. (2009). 2-Aminoethoxydiphenyl-borate (2-APB) increases excitability in pyramidal neurons. *Cell Calcium* **45**, 310–317.
- Haouzi, P., Chenuel, B., and Sonobe, T. (2015). High-dose hydroxocobalamin administered after H<sub>2</sub>S exposure counteracts sulfide-poisoning-induced cardiac depression in sheep. *Clin. Toxicol. (Phila)* **53**, 28–36.
- Hayashi, T., Kagaya, A., Takebayashi, M., Oyamada, T., Inagaki, M., Tawara, Y., Yokota, N., Horiguchi, J., Su, T. P., and Yamawaki, S. (1997). Effect of dantrolene on KCl- or NMDA-induced intracellular Ca<sup>2+</sup> changes and spontaneous Ca<sup>2+</sup> oscillation in cultured rat frontal cortical neurons. *J. Neural Transm. (Vienna)* **104**, 811–824.
- Hodges, M. R., and Richerson, G. B. (2008). Contributions of 5-HT neurons to respiratory control: Neuromodulatory and trophic effects. *Respir. Physiol. Neurobiol.* **164**, 222–232.
- Johnstone, A. F., Gross, G. W., Weiss, D. G., Schroeder, O. H., Gramowski, A., and Shafer, T. J. (2010). Microelectrode arrays: A physiologically based neurotoxicity testing platform for the 21st century. *Neurotoxicology* **31**, 331–350.
- Joshi, D. C., Singh, M., Krishnamurthy, K., Joshi, P. G., and Joshi, N. B. (2011). AMPA induced Ca<sup>2+</sup> influx in motor neurons occurs through voltage gated Ca<sup>2+</sup> channel and Ca<sup>2+</sup> permeable AMPA receptor. *Neurochem. Int.* **59**, 913–921.
- Kim, D.-S., Anantharam, P., Hoffmann, A., Meade, M. L., Grobe, N., Gearhart, J. M., Whitley, E. M., Mahama, B., and Rumbleiha, W. K. (2018). Broad spectrum proteomics analysis of the inferior colliculus following acute hydrogen sulfide exposure. *Toxicol. Appl. Pharmacol.* **355**, 28–42.
- Kim, D. S., Anantharam, P., Padhi, P., Thedens, D. R., Li, G., Gilbreath, E., and Rumbleiha, W. K. (2019). Transcriptomic profile analysis of brain inferior colliculus following acute hydrogen sulfide exposure. *Toxicology* **430**, 152345.
- Konrad-Dalhoff, I., Baunack, A. R., Ramsch, K. D., Ahr, G., Kraft, H., Schmitz, H., Wehrauch, T. R., and Kuhlmann, J. (1991). Effect of the calcium antagonists nifedipine, nitrendipine, nimodipine and nisoldipine on oesophageal motility in man. *Eur. J. Clin. Pharmacol.* **41**, 313–316.
- Kurokawa, Y., Sekiguchi, F., Kubo, S., Yamasaki, Y., Matsuda, S., Okamoto, Y., Sekimoto, T., Fukatsu, A., Nishikawa, H., Kume, T., et al. (2011). Involvement of ERK in NMDA receptor-independent cortical neurotoxicity of hydrogen sulfide. *Biochem. Biophys. Res. Commun.* **414**, 727–732.
- Lopez, J. J., Jardin, I., Sanchez-Collado, J., Salido, G. M., Smani, T., and Rosado, J. A. (2020). TRPC channels in the SOCE scenario. *Cells* **9**, 126.
- Morii, D., Miyagatani, Y., Nakamae, N., Murao, M., and Taniyama, K. (2010). Japanese experience of hydrogen sulfide: The suicide craze in 2008. *J. Occup. Med. Toxicol.* **5**, 28.
- Muramoto, K., Ichikawa, M., Kawahara, M., Kobayashi, K., and Kuroda, Y. (1993). Frequency of synchronous oscillations of neuronal activity increases during development and is correlated to the number of synapses in cultured cortical neuron networks. *Neurosci. Lett.* **163**, 163–165.
- Nam, B., Kim, H., Choi, Y., Lee, H., Hong, E. S., Park, J. K., Lee, K. M., and Kim, Y. (2004). Neurologic sequela of hydrogen sulfide poisoning. *Ind. Health* **42**, 83–87.
- Ng, P. C., Hendry-Hofer, T. B., Witeof, A. E., Brenner, M., Mahon, S. B., Boss, G. R., Haouzi, P., and Bebartha, V. S. (2019). Hydrogen sulfide toxicity: Mechanism of action, clinical presentation, and countermeasure development. *J. Med. Toxicol.* **15**, 287–294.
- Nunez, L., Sanchez, A., Fonteriz, R. I., and Garcia-Sancho, J. (1996). Mechanisms for synchronous calcium oscillations in cultured rat cerebellar neurons. *Eur. J. Neurosci.* **8**, 192–201.
- O'Donoghue, J. G. (1961). Hydrogen sulphide poisoning in swine. *Can. J. Compar. Med. Vet. Sci.* **25**, 217–219.
- Polhemus, D. J., and Lefer, D. J. (2014). Emergence of hydrogen sulfide as an endogenous gaseous signaling molecule in cardiovascular disease. *Circ. Res.* **114**, 730–737.
- Pozsgai, G., Batai, I. Z., and Pinter, E. (2019). Effects of sulfide and polysulfides transmitted by direct or signal transduction-mediated activation of trpa1 channels. *Br. J. Pharmacol.* **176**, 628–645.
- Purnell, B. S., and Buchanan, G. F. (2020). Free-running circadian breathing rhythms are eliminated by suprachiasmatic nucleus lesion. *J. Appl. Physiol.* **129**, 49–57.
- Purnell, B. S., Hajek, M. A., and Buchanan, G. F. (2017). Time-of-day influences on respiratory sequelae following maximal electroshock-induced seizures in mice. *J. Neurophysiol.* **118**, 2592–2600.
- Roa-Coria, J. E., Pineda-Farias, J. B., Barragan-Iglesias, P., Quinonez-Bastidas, G. N., Zuniga-Romero, A., Huerta-Cruz, J. C., Reyes-Garcia, J. G., Flores-Murrieta, F. J., Granados-Soto, V., and Rocha-Gonzalez, H. I. (2019). Possible involvement of peripheral trp channels in the hydrogen sulfide-induced hyperalgesia in diabetic rats. *BMC Neurosci.* **20**, 1.
- Robinson, H. P., Kawahara, M., Jimbo, Y., Torimitsu, K., Kuroda, Y., and Kawana, A. (1993). Periodic synchronized bursting and intracellular calcium transients elicited by low magnesium in cultured cortical neurons. *J. Neurophysiol.* **70**, 1606–1616.
- Rumbleiha, W., Whitley, E., Anantharam, P., Kim, D. S., and Kanthasamy, A. (2016). Acute hydrogen sulfide-induced neuropathology and neurological sequelae: Challenges for translational neuroprotective research. *Ann. N. Y. Acad. Sci.* **1378**, 5–16.
- Samanta, A., Hughes, T. E. T., and Moiseenkova-Bell, V. Y. (2018). Transient receptor potential (TRP) channels. *Subcell Biochem.* **87**, 141–165.
- Santana Maldonado, C., Weir, A., and Rumbleiha, W. K. (2022). A comprehensive review of treatments for hydrogen sulfide poisoning: Past, present, and future. *Toxicol. Mech. Methods* **33**, 183–196.
- Santos, S. F., Pierrot, N., Morel, N., Gailly, P., Sindic, C., and Octave, J. N. (2009). Expression of human amyloid precursor protein in rat cortical neurons inhibits calcium oscillations. *J. Neurosci.* **29**, 4708–4718.
- Sastre, C., Baillif-Couniou, V., Kintz, P., Cirimele, V., Bartoli, C., Christia-Lotter, M. A., Piercecchi-Marti, M. D., Leonetti, G., and Pelissier-Alicot, A. L. (2013). Fatal accidental hydrogen sulfide poisoning: A domestic case. *J. Forensic Sci.* **58**, S280–S284.
- Smedler, E., and Uhlen, P. (2014). Frequency decoding of calcium oscillations. *Biochim. Biophys. Acta.* **1840**, 964–969.
- Smith, J. C., Ellenberger, H. H., Ballanyi, K., Richter, D. W., and Feldman, J. L. (1991). Pre-botzinger complex: A brainstem region that may generate respiratory rhythm in mammals. *Science* **254**, 726–729.
- Sneyd, J., Han, J. M., Wang, L., Chen, J., Yang, X., Tanimura, A., Sanderson, M. J., Kirk, V., and Yule, D. I. (2017). On the dynamical structure of calcium oscillations. *Proc. Natl. Acad. Sci. U.S.A.* **114**, 1456–1461.
- Snyder, J. W., Safir, E. F., Summerville, G. P., and Middleberg, R. A. (1995). Occupational fatality and persistent neurological sequelae after mass exposure to hydrogen sulfide. *Am. J. Emerg. Med.* **13**, 199–203.

- Sombati, S., and Delorenzo, R. J. (1995). Recurrent spontaneous seizure activity in hippocampal neuronal networks in culture. *J. Neurophysiol.* **73**, 1706–1711.
- Sonobe, T., and Haouzi, P. (2015). H<sub>2</sub>S induced coma and cardiogenic shock in the rat: Effects of phenothiazinium chromophores. *Clin. Toxicol.* **53**, 525–539.
- Spletstoeser, F., Florea, A. M., and Busselberg, D. (2007). IP(3) receptor antagonist, 2-APB, attenuates cisplatin induced Ca<sup>2+</sup>-influx in HeLa-S3 cells and prevents activation of calpain and induction of apoptosis. *Br. J. Pharmacol.* **151**, 1176–1186.
- Tanaka, S., Fujimoto, S., Tamagaki, Y., Wakayama, K., Shimada, K., and Yoshikawa, J. (1999). Bronchial injury and pulmonary edema caused by hydrogen sulfide poisoning. *Am. J. Emerg. Med.* **17**, 427–429.
- Tokumitsu, H., and Sakagami, H. (2022). Molecular mechanisms underlying Ca<sup>2+</sup>/calmodulin-dependent protein kinase signal transduction. *Int. J. Mol. Sci.* **23**, 11025.
- Tvedt, B., Edland, A., Skyberg, K., and Forberg, O. (1991a). Delayed neuropsychiatric sequelae after acute hydrogen sulfide poisoning: Affection of motor function, memory, vision and hearing. *Acta Neurol. Scand.* **84**, 348–351.
- Tvedt, B., Skyberg, K., Aaserud, O., Hobbesland, A., and Mathiesen, T. (1991b). Brain damage caused by hydrogen sulfide: A follow-up study of six patients. *Am. J. Ind. Med.* **20**, 91–101.
- Wang, Y., Tang, S., Harvey, K. E., Salyer, A. E., Li, T. A., Rantz, E. K., Lill, M. A., and Hockerman, G. H. (2018). Molecular determinants of the differential modulation of Cav1.2 and Cav1.3 by nifedipine and FPL 64176. *Mol. Pharmacol.* **94**, 973–983.
- Wasch, H. H., Estrin, W. J., Yip, P., Bowler, R., and Cone, J. E. (1989). Prolongation of the P-300 latency associated with hydrogen sulfide exposure. *Arch. Neurol.* **46**, 902–904.
- Xu, W., and Lipscombe, D. (2001). Neuronal Ca(V)1.3α(1) L-type channels activate at relatively hyperpolarized membrane potentials and are incompletely inhibited by dihydropyridines. *J. Neurosci.* **21**, 5944–5951.
- Zheng, J., Yu, Y., Feng, W., Li, J., Liu, J., Zhang, C., Dong, Y., Pessah, I. N., and Cao, Z. (2019). Influence of nanomolar deltamethrin on the hallmarks of primary cultured cortical neuronal network and the role of ryanodine receptors. *Environ Health Perspect* **127**, 67003.